Title
The arc of the Snowball: U-Pb dates constrain the Islay anomaly and the initiation of the Sturtian glaciation

Journal
Geology, 46(6)

ISSN
0091-7613

Authors
MacLennan, Scott
Park, Yuem
Swanson-Hysell, Nicholas
et al.

Publication Date
2018-06-01

DOI
10.1130/g40171.1

Publisher: GSA
Journal: GEOL: Geology
DOI:10.1130/G40171.1

The arc of the Snowball: U-Pb dates constrain the Islay anomaly and the initiation of the Sturtian glaciation

Scott MacLennan[1], Yuem Park[2], Nicholas Swanson-Hysell[2], Adam Maloof[1], Blair Schoene[1], Mulubrhan Gebreslassie[3], Eliel Antilla[2], Tadele Tesema[3], Mulugeta Alene[3], and Bereket Haileab[4]

[1]*Department of Geosciences, Princeton University, Princeton, New Jersey 08544, USA*

[2]*Earth and Planetary Sciences Department, University of California, Berkeley, California 94720, USA*

[3]*School of Earth Sciences, Addis Ababa University, P.O. Box 1176, Addis Ababa, Ethiopia*

[4]*Department of Geology, Carleton College, Northfield, Minnesota 55057, USA*

ABSTRACT

In order to understand the onset of Snowball Earth events, precise geochronology and chemostratigraphy are needed on complete sections leading into the glaciations. While deposits associated with the Neoproterozoic Sturtian glaciation have been found on nearly every continent, time-calibrated stratigraphic sections that record paleoenvironmental conditions leading into the glaciation are exceedingly rare. Instead, the transition to glaciation is normally expressed as erosive contacts with overlying diamictites, and the best existing geochronological constraints come from volcanic successions with little paleoenvironmental information. We report new stratigraphic and geochronological data from the upper Tambien Group in northern Ethiopia, which indicates that the glacigenic diamictite at the top of the succession is Sturtian in age. U-

Pb zircon dates obtained from two tuffaceous siltstones that are 74 and 84 m below the diamictite are 719.68 ± 0.46 Ma and 719.68 ± 0.56 Ma (2σ), respectively. We also report a U-Pb date of 735.25 ± 0.25 Ma from a crystal-rich tuff located 2 m above the nadir of a high-amplitude, basin-wide, negative $\delta^{13}C$ excursion previously correlated with the Islay anomaly. This age for the anomaly agrees with Re-Os age constraints from Laurentia, suggesting that the $\delta^{13}C$ signal is globally synchronous and preceded the Sturtian glaciation by ~18 m.y. The interval between the Islay anomaly and Sturtian glaciation is recorded in the Tambien Group as an ~600 m succession of predominantly shallow-water carbonates and siliciclastics with $\delta^{13}C$ values recording a prolonged period at +5‰, followed by an interval of lower, but still positive, values leading up to the glaciation. Our data are consistent with synchronous global onset of the Sturtian glaciation at ca. 717 Ma. Shallow-water carbonates in strata directly below the first diamictite suggest that glacial onset was rapid in terranes of the Arabian-Nubian Shield.

INTRODUCTION

The two glacial episodes that define the Cryogenian, the Sturtian and Marinoan, are both preceded by large negative $\delta^{13}C$ isotope excursions that have been identified in numerous sections globally (Halverson et al., 2005; Prave et al., 2009). It has been proposed that these excursions have a causal relationship to the onset of glacial conditions, as the $\delta^{13}C$ signals were interpreted to reflect large perturbations to the global carbon cycle (Hoffman et al., 1998; Schrag et al., 2002). It now has been shown that, preceding both the Sturtian and Marinoan Snowball events, carbon isotopes recover from deeply negative values prior to glacial conditions (Halverson et al., 2005; Prave et al., 2009; Rose et al., 2012). Re-Os age constraints place the negative isotope excursion preceding the Sturtian glaciation (Islay anomaly) between739 ± 6 Ma and 732 ± 4 Ma, that is, >15 m.y. before the first diamictites (Rooney et al., 2014; Strauss et al., 2014).

Models for the mechanisms driving Sturtian Snowball initiation include enhanced organic production and remineralization under anaerobic conditions (Tziperman et al., 2011), increased CO_2 sequestration through weathering of large volumes of mafic extrusions at equatorial latitudes (Goddéris et al., 2003; Macdonald et al., 2010), and sulfate injection into the stratosphere caused by equatorial basaltic eruptions (Macdonald and Wordsworth, 2017). Regardless of the initiation mechanism, once ice sheet extent reaches ~30° of latitude, numerical models predict that ice expansion to the equator should occur over thousands of years due to the ice albedo feedback (Baum and Crowley, 2001).

Temporally constrained chemo- and lithostratigraphic records that are continuous into glacial events are critical for testing the Snowball Earth hypothesis and its proposed initiation mechanisms. In this contribution, we present new geochronology and carbonate $\delta^{13}C$ chemostratigraphy from the upper Tambien Group in northern Ethiopia deposited during the lead-up to Sturtian glaciation.

GEOLOGICAL SETTING

The Tambien Group (Tigray Region, northern Ethiopia) is a thick Tonian-Cryogenian carbonate-siliciclastic succession that culminates in diamictite interpreted to have been deposited during the Sturtian 'Snowball Earth' glaciation (Fig. 1; Beyth et al., 2003; Miller et al., 2003, 2009; Swanson-Hysell et al., 2015). The Tambien Group overlies a thick succession of extrusive volcanics and volcaniclastic rocks associated with arc magmatism within the present-day Arabian-Nubian Shield (see the GSA Data

Repository[1] for a geological map). The succession was folded during the East African Orogeny (Stern, 1994; Johnson, 2014), and now is exposed within NNE-trending structures (see the Data Repository).

This study focuses on the upper ~1 km of the Tambien Group (Fig. 1). It begins with the Didikama Formation—extensively dolomitized and recrystallized pale-brown carbonates interbedded with siltstones. This transitions into well-preserved limestone ribbonite (micrite with ribbon-like laminations) with molar tooth structures of the Matheos Formation. Carbonates near the contact between these two formations record a large negative $\delta^{13}C$ excursion to values below −6‰ that was tentatively correlated with the Islay anomaly (Swanson-Hysell et al., 2015), and that we now reproduce in additional sections across the basin (Fig. 1). The ribbonites that record the recovery from the negative anomaly transition into the upper Matheos Formation, which is dominated by oolitic grainstones with abundant molar tooth structures. Dolomitized stromatolites and minor fine-grained siliciclastics serve as a distinctive and consistent marker for the base of the overlying Mariam Bohkahko Formation. The Mariam Bohkahko Formation exhibits two lithofacies that are geographically separated: (1) a dominantly carbonate, or (2) a fine-grained siliciclastic and lesser carbonate lithofacies (Fig. 1). They are interpreted to be temporally synchronous, but reflect different depositional conditions. Where the formation is dominated by carbonate, the lithofacies typically are stromatolitic with intercalated intraclast breccias suggestive of a warm, shallow-water carbonate platform. In the siliciclastic facies–dominated area, the formation is composed of shales and siltstone with allodapic ribbonite and minor grainstone interbeds. Rippled fine

DOI:10.1130/G40171.1

sandstone, oncolite, and carbonate intraclast breccia beds occur at the top of the formation.

Diamictites of the Negash Formation atop the Mariam Bohkahko Formation previously were reported only within the core of the Negash Syncline (see the Data Repository), but new mapping has led to the discovery of exposures of the diamictite and underlying strata near the town of Samre (see the Data Repository for a regional geological map). These exposures significantly expand known exposure of the formation, which is dominated by matrix-supported diamictite with intervals of conglomerate and sandstone. The contact with the underlying Mariam Bohkahko formation is distinct but seemingly conformable. However, in isolated areas within the carbonate-dominated facies, a carbonate conglomerate occurs along the contact, indicating some erosion of the carbonate lithologies did occur and some time may be missing.

Clasts within the diamictite include carbonate lithologies likely sourced from the Tambien Group, volcanic lithologies likely sourced from the basement arc volcanics, and other lithologies such as granite and felsic gneiss that are likely extra-basinal. Striated clasts can be found within the diamictite, which along with stratigraphic arguments, have led to a glacigenic interpretation for the unit (e.g., Miller et al., 2003). The additional exposure near Samre has presented an opportunity to develop further chemostratigraphic and geochronologic constraints on the interval immediately preceding the Sturtian Glaciation.

Existing Geochronological Constraints on Pre-Sturtian Stratigraphy

Glacial sedimentary rocks correlated with the Sturtian glaciation have been reported from most Proterozoic continents (Hoffman and Li, 2009), but few successions

DOI:10.1130/G40171.1

have radiometric age constraints (Figs. 1 and 2). Most sedimentary successions have been assigned a Sturtian age based on chemo- and lithostratigraphic correlations (e.g., Halverson et al., 2005).

A chemical abrasion–isotope dilution–thermal ionization mass spectrometry (CA-ID-TIMS) U-Pb zircon date of 711.5 ± 0.3 Ma (all dates presented with 2σ errors that include analytical uncertainty only) from a volcaniclastic interval within the Ghubrah diamictite of Oman provides a minimum age constraint on the initiation of Sturtian glaciation (Bowring et al., 2007). Two CA-ID-TIMS U-Pb zircon dates of 716.9 ± 0.4 and 717.43 ± 0.14 Ma from volcanic rocks within and below glacial diamictites of the upper Mount Harper Group, northern Laurentia, bracket the onset of low-latitude glaciation (Macdonald et al., 2010, 2017). There is the possibility, however, that these dates represent a minimum age for the onset of the Sturtian, as mafic volcanics underlie the glacial diamictite in this area, and are not the ideal lithology to record glacial influence (Macdonald et al., 2010, 2017). It is therefore important to test these temporal constraints in other successions.

A volcaniclastic sandstone that directly underlies, but is unconformable with, Sturtian diamictite in northern Alaska (USA) yielded a CA-ID-TIMS U-Pb zircon date of 719.47 ± 0.29 Ma (Fig. 2; Cox et al., 2015) that is interpreted as a maximum depositional age. Lower-precision U-Pb secondary ion mass spectrometry analyses (SIMS) on zircons from tuffaceous siltstones from strata preceding Sturtian diamictites in South China have yielded dates of 715.9 ± 2.9 Ma and 716.1 ± 3.4 Ma (Fig. 2; Lan et al., 2014). These dates are within the uncertainty of the ID-TIMS dates from Laurentia (Fig. 2; Macdonald et al., 2010).

The Islay anomaly is a sharp negative $\delta^{13}C$ excursion with a nadir below −6‰ recognized to precede the Sturtian glaciation (Hoffman et al., 2012). The anomaly currently is bracketed stratigraphically by two Re-Os isochron ages of 732.2 ± 4.7 Ma and 739.9 ± 6.1 Ma (2σ errors with all external uncertainties) from Laurentia (Rooney et al., 2014; Strauss et al., 2014). These constraints suggest that the Islay anomaly precedes the Sturtian glaciation by >15 m.y., which negates direct causative links between the $\delta^{13}C$ excursion and the initiation of Snowball Earth events (Hoffman et al., 1998; Schrag et al., 2002; Pavlov et al., 2003; Rothman et al., 2003; Tziperman et al., 2011). Confirming this age difference with another radiometric method from other basins will bolster this conclusion, and test whether the excursion is globally synchronous.

RESULTS AND INTERPRETATION

We identified a number of horizons interpreted to have volcanic input in the Samre area, and sampled them for U-Pb zircon dating. Carbonate samples were also collected for $\delta^{13}C$ analysis (Fig. 1). Two samples (SAM-ET-03 and SAM-ET-04) of light-colored ~25-cm-thick tuffaceous siltstones in the upper Mariam Bohkahko Formation were collected. Details regarding sample location, preparation, and U-Pb analysis are available in the Data Repository. The zircon grains typically were small (c axis <80 μm) and showed signs of metamictization. The analyzed zircons yield ^{238}U-^{206}Pb dates from 840 to 698 Ma. The age spectra are interpreted to indicate the presence of detrital grains. However, both samples show distinct age clusters at ca. 719 Ma that overlap with uncertainties of ~1 m.y. (see the Data Repository). Weighted mean ages of 719.68 ± 0.46 Ma (n = 8) and 719.58 ± 0.56 Ma (n = 3) were calculated for samples SAM-ET-04 and SAM-ET-03, respectively, using these age clusters (Fig. 2). Within the two samples, there are three younger grains that do not overlap with the cluster at ca. 719 Ma (see the Data Repository). While these young zircon dates could indicate that all the grains older than 698 Ma are detrital, we favor the interpretation that the young dates arose from zones of residual Pb loss that escaped chemical abrasion. This interpretation is favored given that these closely stratigraphically spaced samples both have statistically indistinguishable clusters at ca. 719 Ma, while the younger zircons have very different ages, and were not reproduced in 40 single zircon grain analyses. Therefore, we interpret the 719.68 ± 0.46 Ma and 719.58 ± 0.56 Ma dates as eruptive ages that constrain the depositional age of the strata (see the Data Repository for the implications of alternative interpretations noted above).

A couplet of crystal-rich tuffs, 4 and 8 cm thick, and separated by 7 cm, were collected as a single sample (T46–102_2Z) just above the contact between the Didikama and Matheos Formations. The tuffs are within the recovery from the Islay anomaly, as they are 2 m above $\delta^{13}C$ values of –4‰, and within carbonates with $\delta^{13}C$ values of ~0‰. Zircons separated from the sample were translucent and euhedral. Dates from these zircons were confined to between 738 and 735 Ma, indicating a lack of detrital zircon input. The weighted mean date for the sample, 735.25 ± 0.25/0.88 Ma (2σ; without/with external uncertainties), is within uncertainty of the Re-Os isochron dates of 732.2 ± 4.7 Ma and 739.9 ± 6.1 Ma (2σ; including external uncertainties) that are interpreted to bracket the Islay anomaly (Rooney et al., 2014; Strauss et al., 2014). Independent Re-Os and U-Pb age constraints now indicate that the deeply negative Islay isotope anomaly is globally synchronous and precedes the Sturtian glaciation by ~18 m.y. The integrated chemostratigraphy and geochronology now confirm that the Tambien basin uniquely

DOI:10.1130/G40171.1

records a prolonged $\delta^{13}C$ +5‰ plateau preserved in the Matheos and lower most Mariam Bohkahko Formations, followed by less positive values (~+2‰), prior to deposition of the first diamictites (Fig. 1).

DISCUSSION

The two dates near the contact with the Negash Formation diamictite confirm the interpretation that the Negash diamictite is Sturtian in age as originally proposed by Beyth et al., (2003). These dates provide new constraints on the timing of initiation of the Sturtian glaciation in the Arabian-Nubian Shield to be after ca. 719 Ma. By making the assumption that sediment accumulation rate over long timescales was controlled by regional subsidence, and therefore remained relatively constant, the timing of glacial onset can be better approximated. Monte Carlo simulations taking into account age and stratigraphic thickness uncertainty were used to calculate sediment accumulation rates between samples T46–102_2Z and SAM-ET-03/SAM-ET-04. Using these rates, we estimated the time represented by the stratal thickness of 74 m between the SAM-ET-04 tuff and the first diamictite. While short-term sedimentation rates will vary considerably with lithofacies, these variations are muted over the million-year timescales in this study. The simulations yield a median age for the base of the diamictite of 717.1 +0.7/–0.9 Ma (95% confidence interval; Fig. 2). This estimated age falls between existing maximum and minimum age constraints on the onset of Sturtian glaciation in Laurentia (Fig. 2; Macdonald et al., 2010, 2017), and is therefore consistent with global synchronicity of glacial initiation, as predicted at low latitudes by the Snowball Earth hypothesis.

The calculated sediment accumulation rates can also be used to estimate the duration of the Islay anomaly. The duration from the initiation of the downturn in $\delta^{13}C$

values through the nadir, to values below −6‰, to the recovery to ~5‰ is implied to be between 0.7 and 1 m.y. In other successions, the recovery of $\delta^{13}C$ values from the nadir of the Islay anomaly is variably truncated by overlying glacial deposits such that they reach −3‰ in the Akademikerbreen Group of Svalbard (Hoffman et al., 2012), 1‰ in the Appin Group of Scotland (Prave et al., 2009), and >5‰ in the Coates Lake Group of northwest Canada (Rooney et al., 2014). The Tambien Group data reproduce the recovery to >5‰ values following the Islay anomaly and show that the plateau of values at ~5‰ was sustained for millions of years prior to Sturtian glaciation (Fig. 1). As evidenced by these data and previous age constraints (Rooney et al., 2014), the mechanism driving $\delta^{13}C$ in carbonate down to ~−6‰ is therefore temporally unrelated to the Sturtian Snowball Earth. In contrast, the upper Mariam Bohkahko Formation records a longer-term trend toward slightly positive $\delta^{13}C$ values directly below the diamictite, making it the most continuous chemostratigraphic record prior to the Sturtian glaciation yet discovered.

Our age model for the Mariam Bohkahko Formation, coupled with the presence of substantial stromatolitic carbonate and beds of oncoids in sediments directly below the diamictite, suggests that conditions remained warm enough to sustain shallow-water carbonate production until just prior to the deposition of glacial diamictite. This interpretation implies that the transition to low-latitude glaciation was rapid—consistent with the Snowball Earth hypothesis.

CONCLUSIONS

A U-Pb zircon age within the sharp recovery from a deeply negative $\delta^{13}C$ excursion in the upper Tambien Group overlaps with existing Re-Os isochron ages for the Islay anomaly in Laurentia, implying that it is globally synchronous. These dates demonstrate that the Islay anomaly precedes the Sturtian Snowball Earth by >18 m.y., and that there is no direct causative link between the carbon cycle perturbation that caused the excursion and the initiation of low-latitude glaciation. U-Pb zircon dates from strata just below the upper Tambien Group diamictite confirm that it is Sturtian in age. The ages are consistent with global synchronicity of Sturtian glacial sediments and rapid onset of Snowball Earth conditions at ca. 717 Ma.

ACKNOWLEDGMENTS

This research was partially funded by National Science Foundation grants EAR-1325230 (Maloof) and EAR-1323158 (Swanson-Hysell). Robert Bussert alerted the authors to the possible presence of Neoproterozoic diamictite in the Samre area. Carol Dehler and anonymous reviewers are thanked for valuable feedback.

REFERENCES CITED

Baum, S.K., and Crowley, T.J., 2001, GCM response to late Precambrian (~590 Ma) ice-covered continents: Geophysical Research Letters, v. 28, p. 583–586, https://doi.org/10.1029/2000GL011557.

Beyth, M., Avigad, D., Wetzel, H.U., Matthews, A., and Berhe, S.M., 2003, Crustal exhumation and indications for Snowball Earth in the East African Orogen: North Ethiopia and East Eritrea: Precambrian Research, v. 123, p. 187–201, https://doi.org/10.1016/S0301-9268(03)00067-6.

Bowring, S.A., Grotzinger, J.P., Condon, D.J., Ramezani, J., Newall, M.J., and Allen, P.A., 2007, Geochronologic constraints on the chronostratigraphic framework of the neoproterozoic Huqf Supergroup, Sultanate of Oman: American Journal of Science, v. 307, p. 1097–1145, https://doi.org/10.2475/10.2007.01.

Cox, G.M., Strauss, J.V., Halverson, G.P., Schmitz, M.D., McClelland, W.C., Stevenson, R.S., and Macdonald, F.A., 2015, Kikiktat volcanics of Arctic Alaska—Melting of harzburgitic mantle associated with the Franklin large igneous province: Lithosphere, v. 7, p. 275–295, https://doi.org/10.1130/L435.1.

Goddéris, Y., Donnadieu, Y., Nédélec, A., Dupré, B., Dessert, C., Grard, A., Ramstein, G., and François, L.M., 2003, The Sturtian "snowball" glaciation: Fire and ice: Earth and Planetary Science Letters, v. 211, p. 1–12, https://doi.org/10.1016/S0012-821X(03)00197-3.

Halverson, G.P., Hoffman, P.F., Schrag, D.P., Maloof, A.C., and Rice, A.H.N., 2005, Toward a Neoproterozoic composite carbon-isotope record: Geological Society of America Bulletin, v. 117, p. 1181–1207, https://doi.org/10.1130/B25630.1.

Hoffman, P.F., Halverson, G.P., Domack, E.W., Maloof, A.C., Swanson-Hysell, N.L., and Cox, G.M., 2012, Cryogenian glaciations on the southern tropical paleomargin of Laurentia (NE Svalbard and East Greenland), and a primary origin for the upper Russøya (Islay) carbon isotope excursion: Precambrian Research, v. 206–207, p. 137–158, https://doi.org/10.1016/j.precamres.2012.02.018.

Hoffman, P.F., Kaufman, A.J., Halverson, G.P., and Schrag, D.P., 1998, A Neoproterozoic Snowball Earth: Science, v. 281, p. 1342–1346, https://doi.org/10.1126/science.281.5381.1342.

Hoffman, P.F., and Li, Z.X., 2009, A palaeogeographic context for Neoproterozoic glaciation: Palaeogeography, Palaeoclimatology, Palaeoecology, v. 277, p. 158–172, https://doi.org/10.1016/j.palaeo.2009.03.013.

Johnson, P.R., 2014, An expanding Arabian-Nubian Shield geochronologic and isotopic dataset : Defining limits and confirming the tectonic setting of a Neoproterozoic Accretionary Orogen: The Open Geological Journal, v. 8, p. 3–33, https://doi.org/10.2174/1874262901408010003.

Lan, Z., Li, X., Zhu, M., Chen, Z.Q., Zhang, Q., Li, Q., Lu, D., Liu, Y., and Tang, G., 2014, A rapid and synchronous initiation of the wide spread Cryogenian glaciations: Precambrian Research, v. 255, p. 401–411, https://doi.org/10.1016/j.precamres.2014.10.015.

Macdonald, F.A., and Wordsworth, R., 2017, Initiation of Snowball Earth with volcanic sulfur aerosol emissions: Geophysical Research Letters, v. 44, p. 1938–1946, https://doi.org/10.1002/2016GL072335.

Macdonald, F.A., Schmitz, M.D., Crowley, J.L., Roots, C.F., Jones, D.S., Maloof, A.C., Strauss, J.V., Cohen, P.A., Johnston, D.T., and Schrag, D.P., 2010, Calibrating the Cryogenian: Science, v. 327, p. 1241–1243, https://doi.org/10.1126/science.1183325.

Macdonald, F.A., Schmitz, M.D., Strauss, J.V., Halverson, G.P., Gibson, T.M., Eyster, A., Cox, G., Mamrol, P., and Crowley, J.L., 2017, Cryogenian of Yukon: Precambrian Research, https://doi.org/10.1016/j.precamres.2017.08.015 (in press).

Miller, N.R., Alene, M., Sacchi, R., Stern, R.J., Conti, A., Kröner, A., and Zuppi, G., 2003, Significance of the Tambien Group (Tigrai, N. Ethiopia) for Snowball Earth events in the Arabian-Nubian Shield: Precambrian Research, v. 121, p. 263–283, https://doi.org/10.1016/S0301-9268(03)00014-7.

Miller, N.R., Stern, R.J., Avigad, D., Beyth, M., and Schilman, B., 2009, Cryogenian slate-carbonate sequences of the Tambien Group, Northern Ethiopia (I): Pre-“Sturtian” chemostratigraphy and regional correlations: Precambrian Research, v. 170, p. 129–156, https://doi.org/10.1016/j.precamres.2008.12.004.

Pavlov, A.A., Hurtgen, M.T., Kasting, J.F., and Arthur, M.A., 2003, Methane-rich Proterozoic atmosphere?: Geology, v. 31, p. 87, https://doi.org/10.1130/0091-7613(2003)031<0087:MRPA>2.0.CO;2.

Prave, A.R., Fallick, A.E., Thomas, C.W., and Graham, C.M., 2009, A composite C-isotope profile for the Neoproterozoic Dalradian Supergroup of Scotland and Ireland: Journal of the Geological Society, v. 166, p. 845–857, https://doi.org/10.1144/0016-76492008-131.

Rooney, A.D., Macdonald, F.A., Strauss, J.V., Dudás, F.Ö., Hallmann, C., and Selby, D., 2014, Re-Os geochronology and coupled Os-Sr isotope constraints on the Sturtian snowball Earth: Proceedings of the National Academy of Sciences of the United States of America, v. 111, p. 51–56, https://doi.org/10.1073/pnas.1317266110.

Rose, C.V., Swanson-Hysell, N.L., Husson, J.M., Poppick, L.N., Cottle, J.M., Schoene, B., and Maloof, A.C., 2012, Constraints on the origin and relative timing of the Trezona $\delta^{13}C$ anomaly below the end-Cryogenian glaciation: Earth and Planetary Science Letters, v. 319–320, p. 241–250, https://doi.org/10.1016/j.epsl.2011.12.027.

Rothman, D.H., Hayes, J.M., and Summons, R.E., 2003, Dynamics of the Neoproterozoic carbon cycle: Proceedings of the National Academy of Sciences of the United States of America, v. 100, p. 8124–8129, https://doi.org/10.1073/pnas.0832439100.

Schrag, D.P., Berner, R.A., Hoffman, P.F., and Halverson, G.P., 2002, On the initiation of a snowball Earth: Geochemistry Geophysics Geosystems, v. 3, p. 1–21, https://doi.org/10.1029/2001GC000219.

Stern, R.J., 1994, Arc assembly and continental collision in the Neoproterozoic East African orogen: Implications for the Consolidation of Gondwanaland: Annual Review of Earth and Planetary Sciences, v. 22, p. 319–351, https://doi.org/10.1146/annurev.ea.22.050194.001535.

Strauss, J.V., Rooney, A.D., MacDonald, F.A., Brandon, A.D., and Knoll, A.H., 2014, 740 Ma vase-shaped microfossils from Yukon, Canada: Implications for neoproterozoic chronology and biostratigraphy: Geology, v. 42, p. 659–662, https://doi.org/10.1130/G35736.1.

Swanson-Hysell, N.L., Maloof, A.C., Condon, D.J., Jenkin, G.R.T., Alene, M., Tremblay, M.M., Tesema, T., Rooney, A.D., and Haileab, B., 2015, Stratigraphy and geochronology of the Tambien Group, Ethiopia: Evidence for globally synchronous carbon isotope change in the Neoproterozoic: Geology, v. 43, p. 323–326, https://doi.org/10.1130/G36347.1.

Tziperman, E., Halevy, I., Johnston, D.T., Knoll, A.H., and Schrag, D.P., 2011, Biologically induced initiation of Neoproterozoic snowball-Earth events: Proceedings of the National Academy of Sciences of the United States of America, v. 108, p. 15091–15096, https://doi.org/10.1073/pnas.1016361108.

FIGURE CAPTIONS

Figure 1. A: Simplified lithostratigraphic columns summarizing the stratigraphic and geochronological constraints on successions deposited before and during the Sturtian glaciation from the South China craton, Laurentia, Oman, and the Arabian-Nubian Shield (Samre, northern Ethiopia) (including 2σ internal uncertainties). B: $\delta^{13}C$ values from carbonates and geochronological constraints (including all external uncertainties) from pre-Sturtian successions. Fm.—Formation, Grp.—Group, SIMS—secondary ion mass spectrometry, ID-TIMS—isotope dilution–thermal ionization mass spectrometry.

Figure 2. U-Pb date distribution plots of dates constraining the age of the initiation of Sturtian glaciation (2σ internal uncertainties). Histogram shows the distribution of estimated ages for the initiation of glacial sedimentation in the Tambien Group estimated with the Monte Carlo method, with the dashed orange lines showing the bounds for 95% of the estimates. Data sources are Bowring et al. (2007), Macdonald et al. (2010), Lan et al. (2014), and Macdonald et al., 2017). Grp.—Group.

[1]**GSA Data Repository item 2018176, description and photographs/micrographs of carbonate lithofacies and geochronological samples, as well as geochronological and chemostratigraphic methodologies and datasets, is available online at http://www.geosociety.org/datarepository/2018/ or on request from editing@ geosociety.org.**

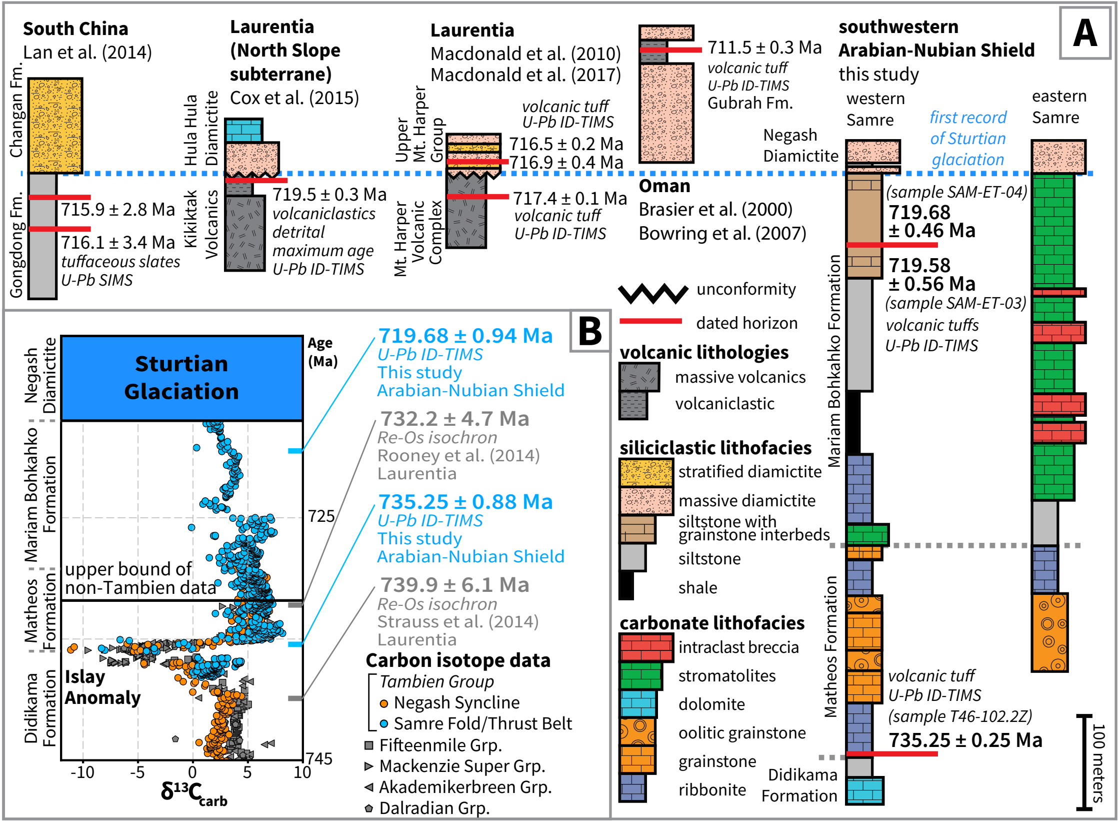

A
South China
Lan et al. (2014)
Changan Fm.
Gongdong Fm.
715.9 ± 2.8 Ma
716.1 ± 3.4 Ma
tuffaceous slates
U-Pb SIMS
Laurentia
(North Slope subterrane)
Cox et al. (2015)
Hula Hula Diamictite
Kikiktak Volcanics
719.5 ± 0.3 Ma
volcaniclastics
detrital
maximum age
U-Pb ID-TIMS
Laurentia
Macdonald et al. (2010)
Macdonald et al. (2017)
Upper Mt. Harper Group
Mt. Harper Volcanic Complex
volcanic tuff
U-Pb ID-TIMS
716.5 ± 0.2 Ma
716.9 ± 0.4 Ma
717.4 ± 0.1 Ma
volcanic tuff
U-Pb ID-TIMS
711.5 ± 0.3 Ma
volcanic tuff
U-Pb ID-TIMS
Gubrah Fm.
Oman
Brasier et al. (2000)
Bowring et al. (2007)
southwestern
Arabian-Nubian Shield
this study
western
Samre
eastern
Samre
first record
of Sturtian
glaciation
Negash
Diamictite
(sample SAM-ET-04)
719.68
± 0.46 Ma
719.58
± 0.56 Ma
(sample SAM-ET-03)
volcanic tuffs
U-Pb ID-TIMS
Mariam Bohkahko Formation
Matheos Formation
volcanic tuff
U-Pb ID-TIMS
(sample T46-102.2Z)
735.25 ± 0.25 Ma
Didikama
Formation
100 meters
unconformity
dated horizon
volcanic lithologies
massive volcanics
volcaniclastic
siliciclastic lithofacies
stratified diamictite
massive diamictite
siltstone with
grainstone interbeds
siltstone
shale
carbonate lithofacies
intraclast breccia
stromatolites
dolomite
oolitic grainstone
grainstone
ribbonite
B
Sturtian
Glaciation
Negash Diamictite
Mariam Bohkahko Formation
Matheos Formation
Didikama Formation
upper bound of
non-Tambien data
Islay
Anomaly
Age
(Ma)
725
745
-10
-5
0
5
10
δ13Ccarb
719.68 ± 0.94 Ma
U-Pb ID-TIMS
This study
Arabian-Nubian Shield
732.2 ± 4.7 Ma
Re-Os isochron
Rooney et al. (2014)
Laurentia
735.25 ± 0.88 Ma
U-Pb ID-TIMS
This study
Arabian-Nubian Shield
739.9 ± 6.1 Ma
Re-Os isochron
Strauss et al. (2014)
Laurentia
Carbon isotope data
Tambien Group
Negash Syncline
Samre Fold/Thrust Belt
Fifteenmile Grp.
Mackenzie Super Grp.
Akademikerbreen Grp.
Dalradian Grp.

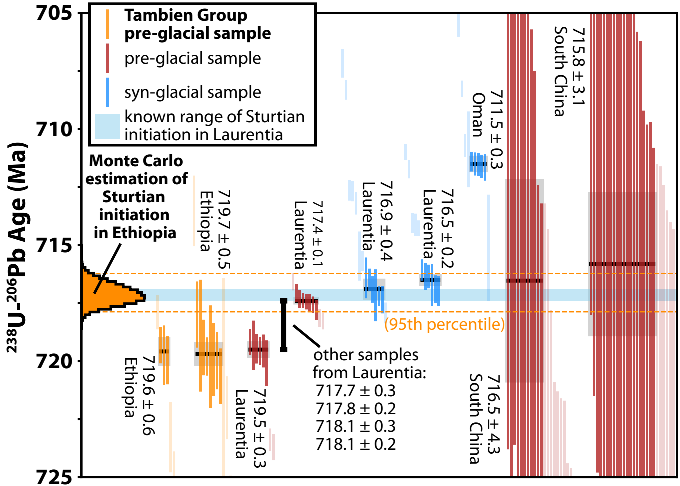

Tambien Group pre-glacial sample
pre-glacial sample
syn-glacial sample
known range of Sturtian initiation in Laurentia
Monte Carlo estimation of Sturtian initiation in Ethiopia
^{238}U-^{206}Pb Age (Ma)
705
710
715
720
725
719.7 ± 0.5 Ethiopia
719.6 ± 0.6 Ethiopia
719.5 ± 0.3 Laurentia
717.4 ± 0.1 Laurentia
716.9 ± 0.4 Laurentia
716.5 ± 0.2 Laurentia
711.5 ± 0.3 Oman
715.8 ± 3.1 South China
716.5 ± 4.3 South China
(95th percentile)
other samples from Laurentia:
717.7 ± 0.3
717.8 ± 0.2
718.1 ± 0.3
718.1 ± 0.2

Data Repository Materials for "The arc of the Snowball: U-Pb dates constrain the Islay anomaly and the initiation of the Sturtian glaciation"

Field area map and lithofacies/sample photos

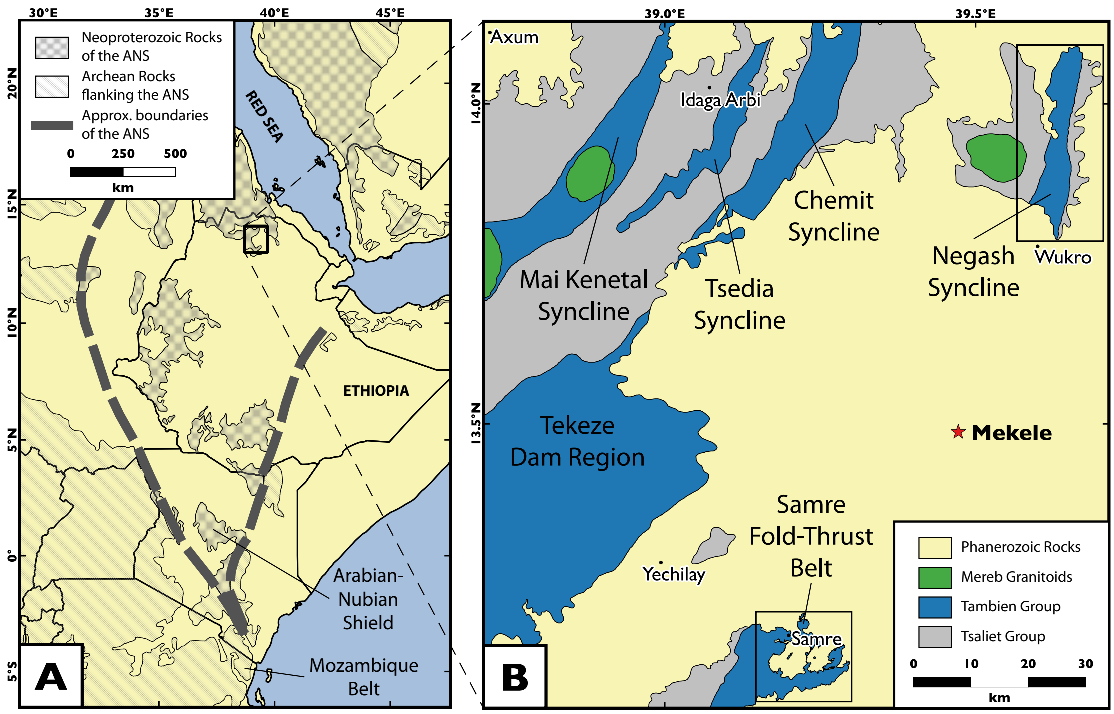

Figure 1. **A) Geological overview map for a portion of the horn of Africa and the Arabian Peninsula showing extent of rocks associated with the Neoproterozoic Arabian-Nubian Shield. B) Simplified geological map for a portion of northern Ethiopia showing the exposures of the Tsaliet and Tambien Groups. The location of the Samre fold and thrust belt where the new geochronological and stratigraphic constrains were obtained is shown..**

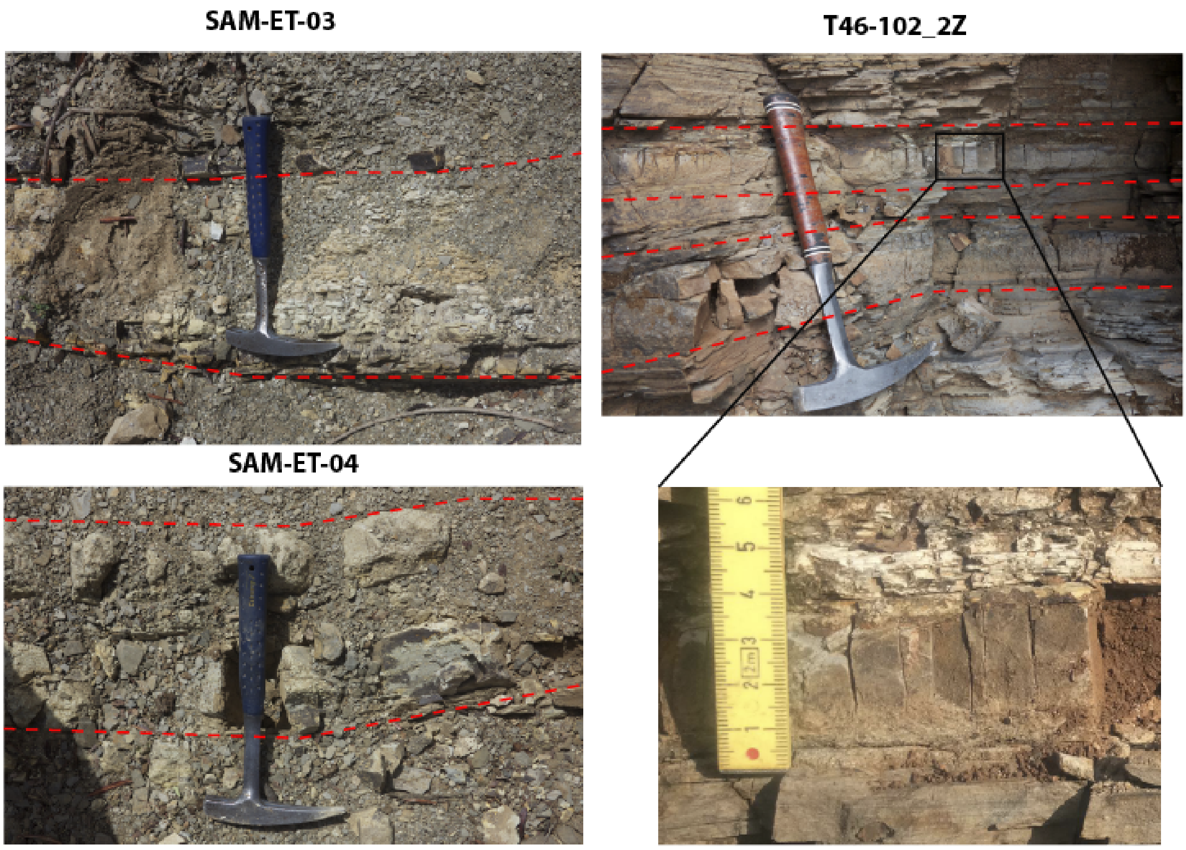

Figure 2. **Sample photographs for the three tuffs dated in this study. SAM-ET-03 and SAM-ET-04 are fine-grained and pale whitish-yellow with a slightly silicified appearance. The crystal tuff couplet sampled as T46-102_2Z had weathered-out calcite veins that indicate a rheological contrast between the tuff and surrounding ribbonite during deformation. A crystal rich zone which fines upward within the tuff can be seen at the base of the ruler in the inset.**

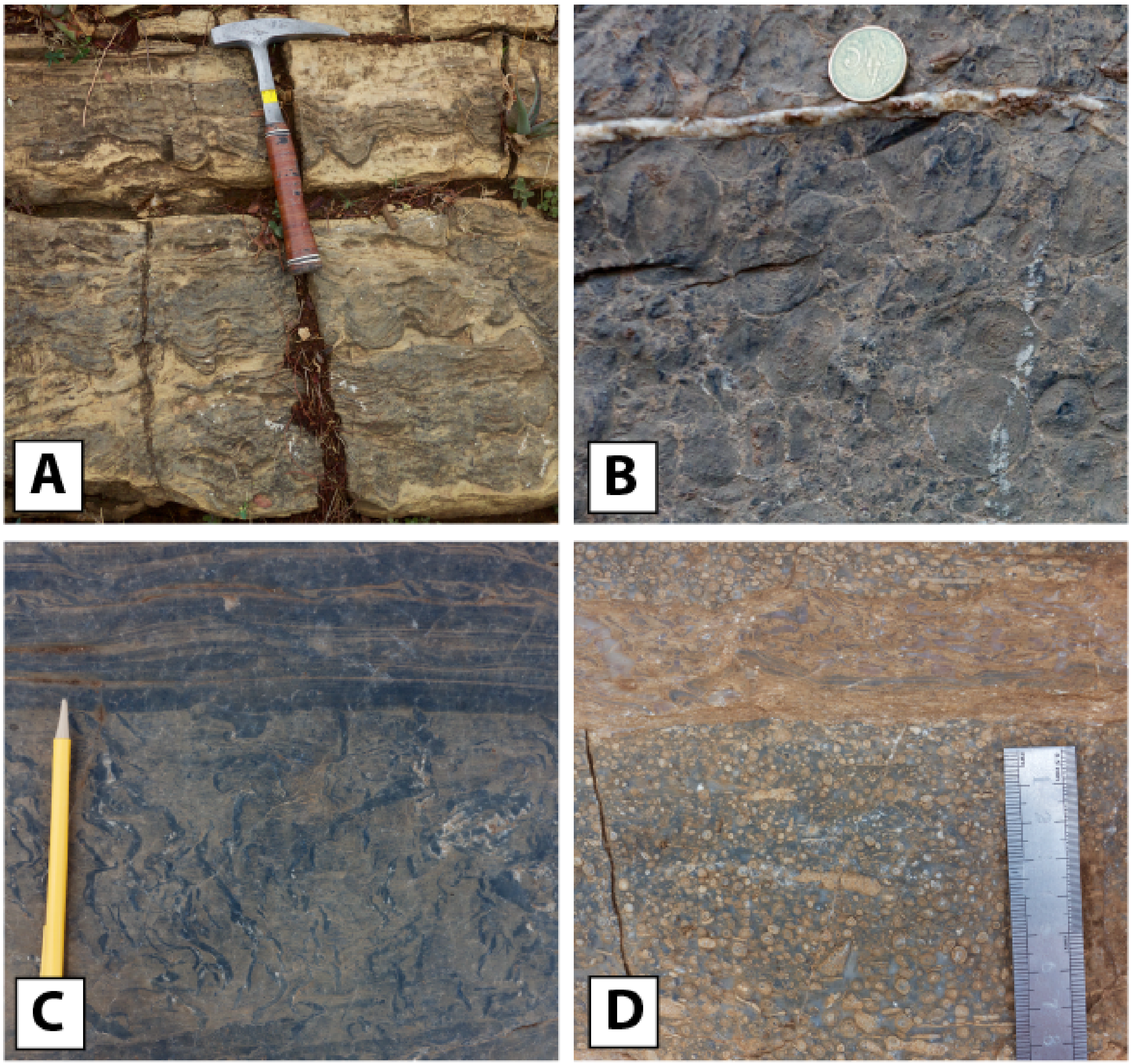

Figure 3. A) Stromatolites (overturned in the photograph) characteristic of the Matheos-Mariam Bohkahko Formation transition. B) Oncolite from the upper Mariam Bohkahko Formation 23 meters below the Negash Formation diamictite. Oncoids are up to 3 cm in diameter, and are cored by carbonate grains and shale rip-up clasts. The 5 birr cent coin used for scale is 2 cm in diameter. C) Molar tooth structures and ribbonite characteristic of the Matheos Formation. D) Oolite with carbonate rip-up clasts (including clasts of ooilite) with an intervening horizon of grainstone with molar teeth structures. The large divisions on the ruler shown for scale are 1 cm. All photos are from the Samre fold-thrust belt.

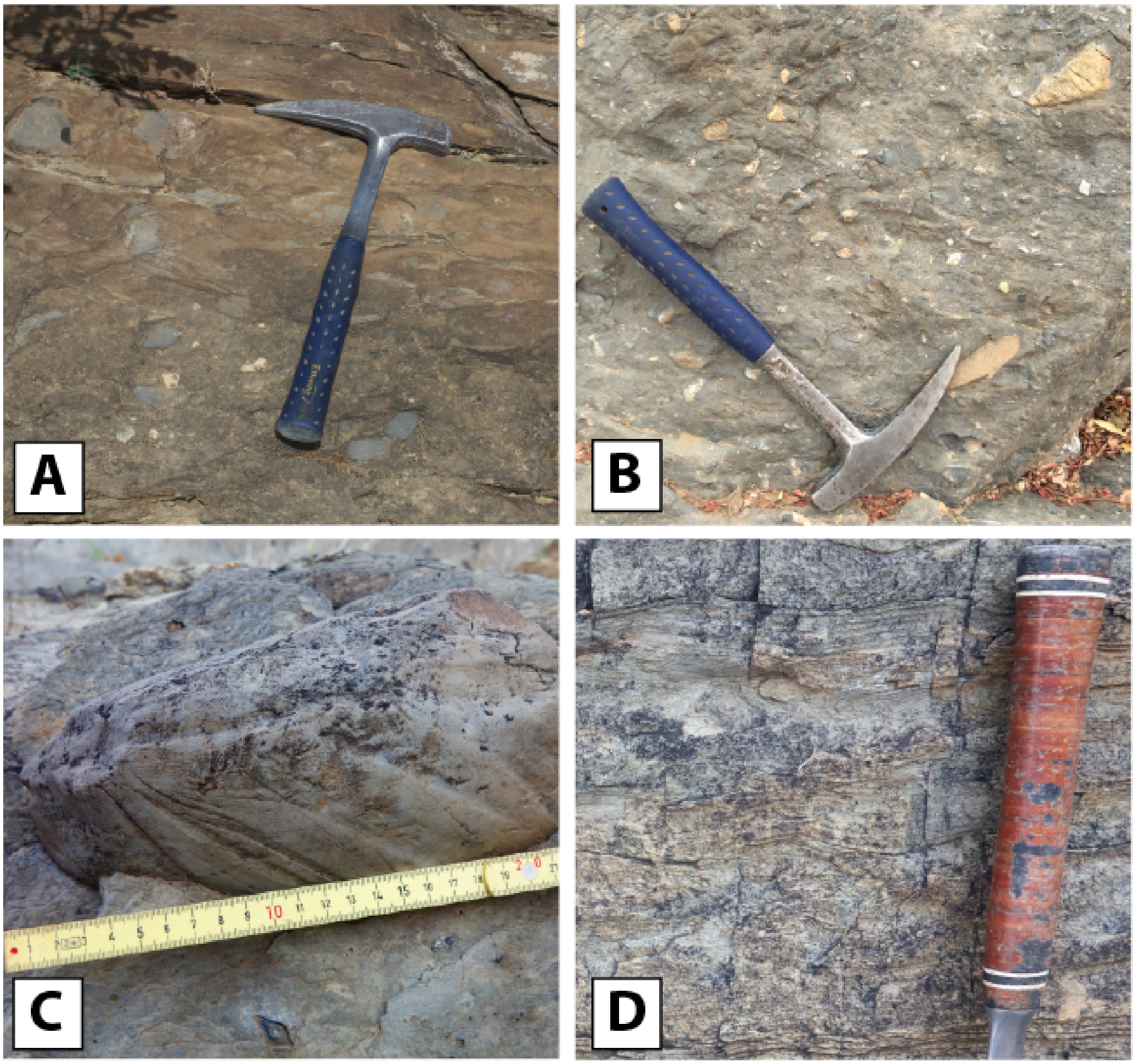

Figure 4. Grainstone with carbonate rip-up clasts from the upper Mariam Bohkahko Formation within 5 m of the diamictite. B) Negash diamictite with subangular clasts of carbonate and metavolcanic rocks. C) Striated quartzite clast within the Negash diamictite. D) Climbing ripples in fine sandstone from the upper Mariam Bohkahko Formation. All photos are from the Samre fold-thrust belt.

Thin section photomicrographs

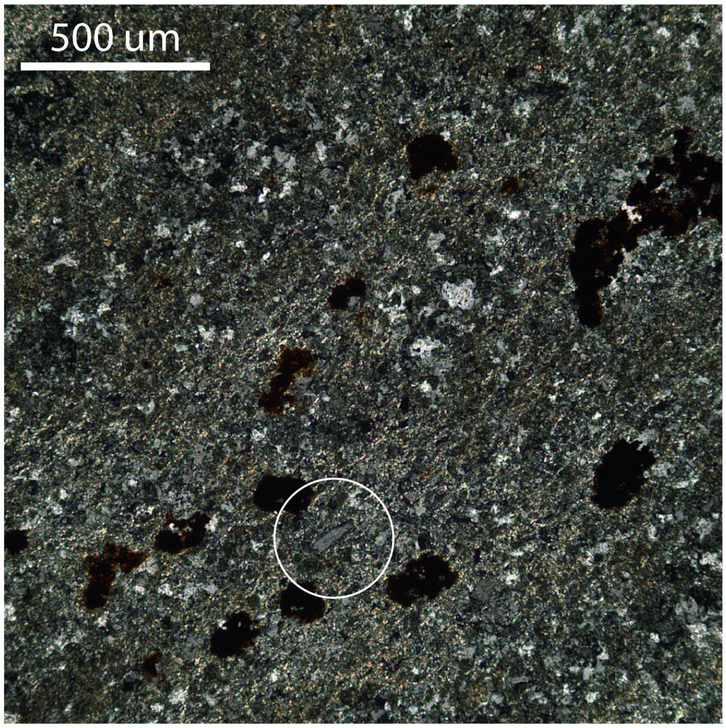

Figure 5. **Cross polarized image of a thin section of the SAM-ET-03 sample. The sample is primarily composed of fine-grained silt and clay, with subangular to subrounded quartz. Angular quartz grains are also visible (one shown with a white circle), which along with the euhedral zircons is suggestive of volcanic input.**

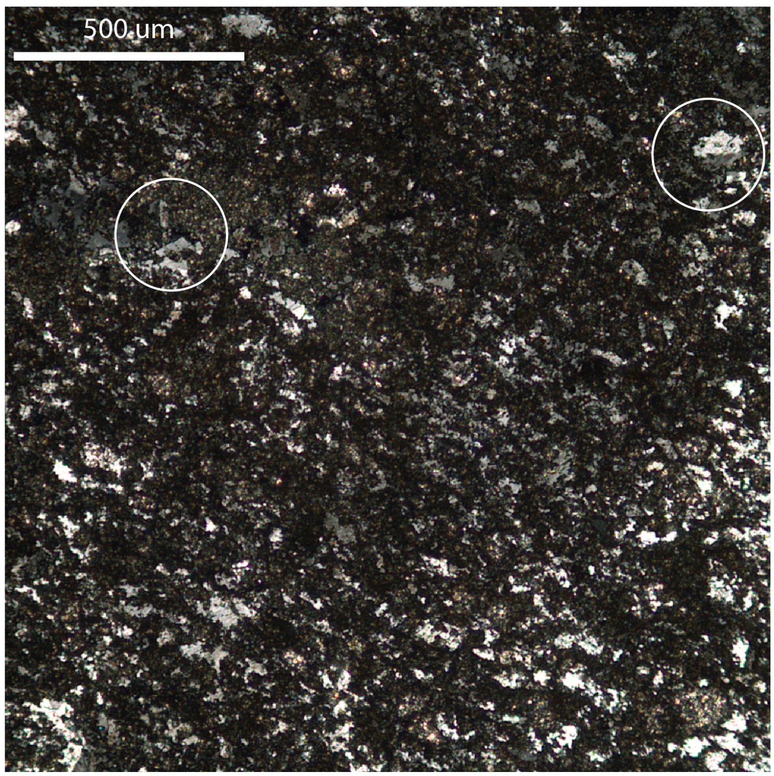

Figure 6. **Cross polarized image of a thin section of sample SAM-ET-04. Similar to sample SAM-ET-03 this sample is predominantly composed of fine siliciclastic grains, but there are again angular quartz grains (white circles) suggestive of volcanic input.**

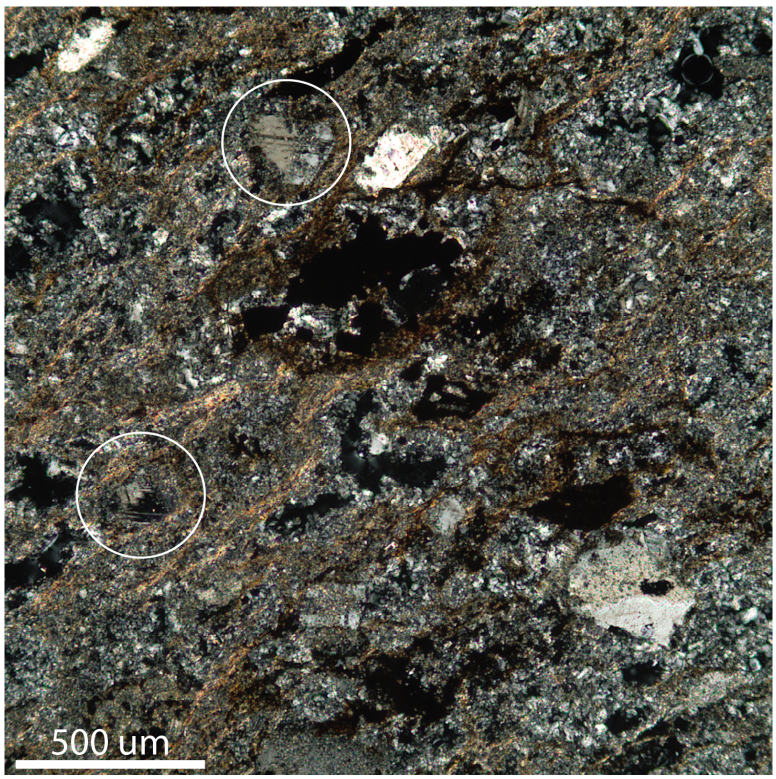

Figure 7. Cross polarized image of a thin section of sample T46-102_2Z. This sample has abundant euhedral quartz and feldspar grains within a fine grained matrix indicating that it is a tuff with minimal reworing.

Zircon photomicrographs

Figure 8. Photomicrographs of zircon grains from samples SAM-ET-04. Grains with a red border were used for the weighted mean age.

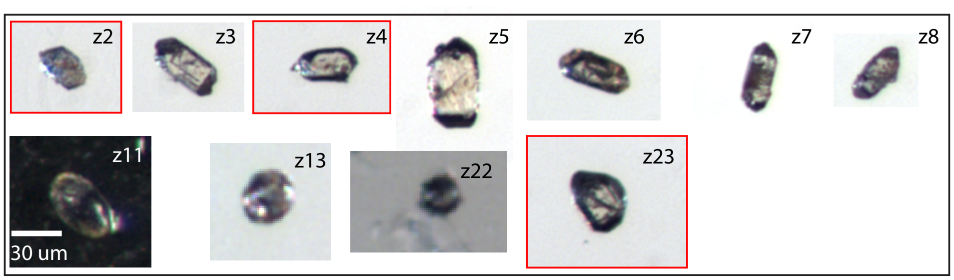

Figure 9. Photomicrographs of zircon grains from samples SAM-ET-03. Grains with a red border were used for the weighted mean age.

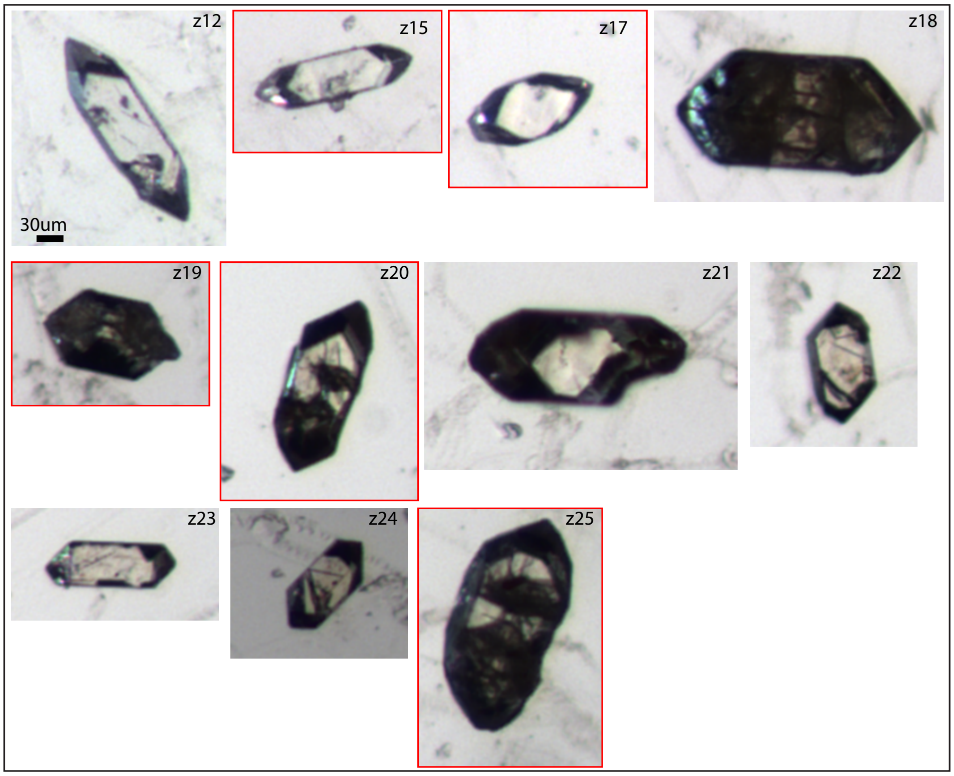

Figure 10. Photomicrographs of zircon grains from samples T46-102_2Z. Grains with a red border were used for the weighted mean age.

U-Pb zircon geochronology methods

Zircons were extracted from rock samples at Princeton University by crushing using a Bico Braun jawcrusher and disc mill, followed by heavy liquid and magnetic separation using methylene iodide and a Frantz isodynamic separator. Zircons were transferred to quartz crucibles and then annealed at 900°C for 48 to 60 hours. Individual zircons were then selected for U-Pb isotope analysis and photographed before transferring them to PFA hex beakers in distilled acetone.

Zircons were then transferred to 200 μL Savillex micro-capsules using distilled acetone. The micro-capsules were then dried down before adding 100 μL 29 M HF and 15 μL 3N HNO_3 to perform chemical abrasion during which the capsules were placed in a high pressure Parr bomb in an oven at 195°C for 12 hours. This process selectively dissolves portions of zircons that have undergone radiation damage and associated Pb loss. Following chemical abrasion, the zircons were rinsed with 6N HCl, HNO_3, and MQ water. The zircons were then spiked with either the single or double EARTHTIME spike containing ^{202}Pb, ^{205}Pb, ^{233}U and ^{235}U, and 100 μL 29 M HF and 15 μL 3N HNO_3 were added prior to full dissolution in a Parr bomb at 210°C for 48 to 60 hours. After dissolution, the aliquots were dried down and converted to chlorides at 195°C for 12 hours. The 6N HCl solutions were dried down and redissolved in 50 μL of 3N HCl prior to ion separation via anion exchange chromatography using 50 μL columns with AG-1 X8 resin. Eichrom 200-400 mesh chloride form resin was used.

The U and Pb washes were dried down with a microdrop of 0.05M H_3PO_4. The dried down U and Pb aliquots were then redissolved in a silica gel emitter (Gerstenberger and Haase, 1997) and deposited on outgassed filaments of zone refined Re. U and Pb isotopic abundances were then measured using an IsotopX PhoeniX-62 TIMS at Princeton University. Pb analyses were either performed in peak-hopping mode on a Daly photonmultiplier ion counting detector, or in peak hopping mode using Faraday cups and Daly photonmultiplier depending on the signal intensity of the sample and spike. U was measured in oxide form, and isotopic abundances were measured using either static measurements on faraday cups with 1012 ohm resistors, or through peak hopping on the Daly photonmultiplier if the sample beam intensity was weak. The Pb and U deadtime characteristics of the Daly photonmultiplier were monitored by running standards (NBS982 and CRM U500) on a weekly basis.

U-Pb Concordia diagrams

Table 1. Summary table of U-Pb data with internal and external uncertainties. 2σ uncertainties are reported in the format ± X/Y/Z, where X is the analytical uncertainty, Y includes uncertainty in the EARTHTIME isotopic tracer, and Z includes uncertainty in the ^{238}U decay constant. MSWD - mean square of weighted deviates.

SAMPLE	$^{206}Pb/^{238}U$ AGE
SAM-ET-03	719.58 ± 0.56/0.64/1.0 (MSWD = 0.54, n = 3)
SAM-ET-04	719.68 ± 0.46/0.54/0.94 (MSWD = 1.3, n = 8)
T46-102_2Z	735.25 ± 0.25/0.39/0.88 (MSWD = 0.36, n = 5)

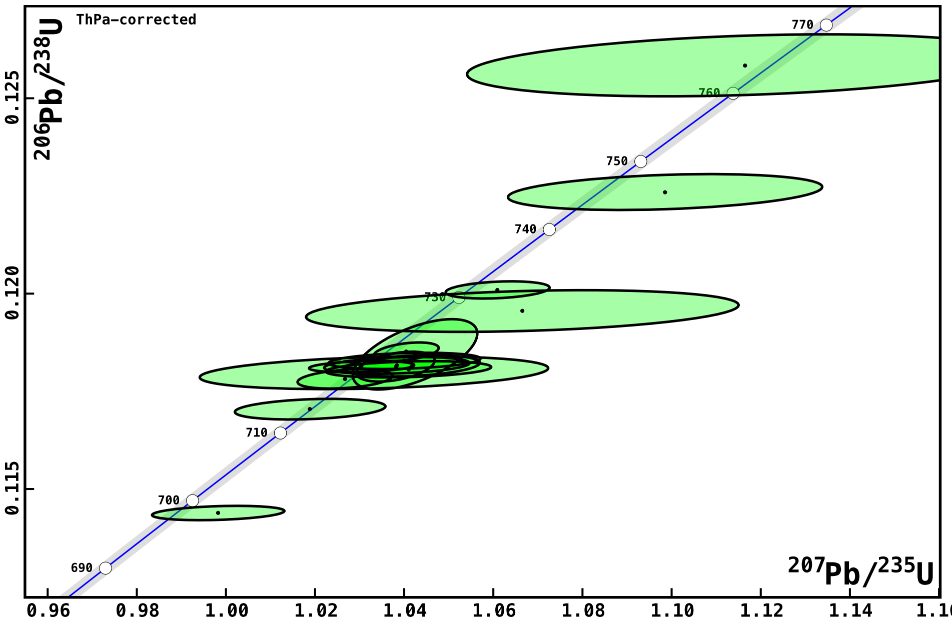

Figure 11. Concordia diagram for SAM-ET-04 showing all the analyses

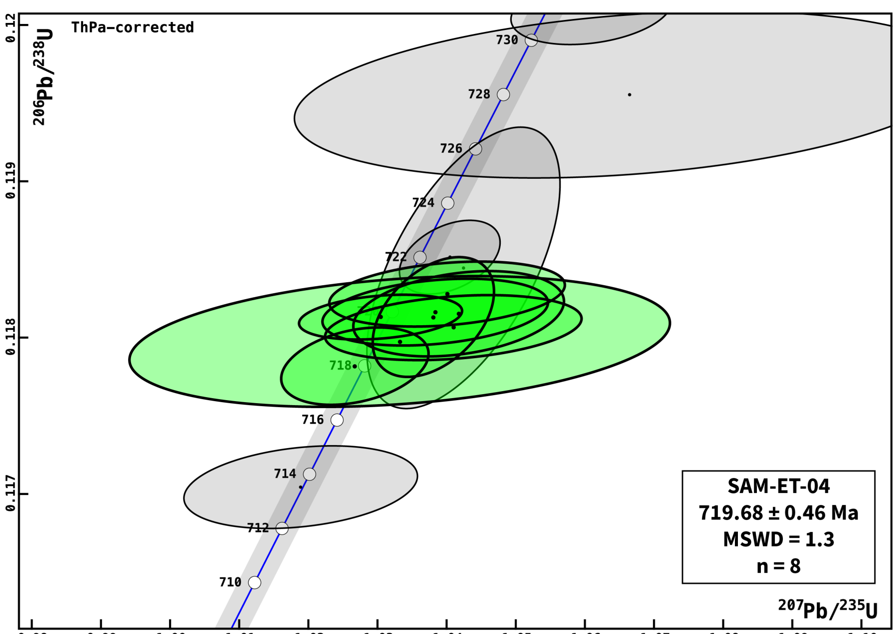

Figure 12. Zoomed-in concordia diagram for SAM-ET-04. The weighted mean date with associated statistical parameters for the sample is shown (2σ analytical uncertainty).

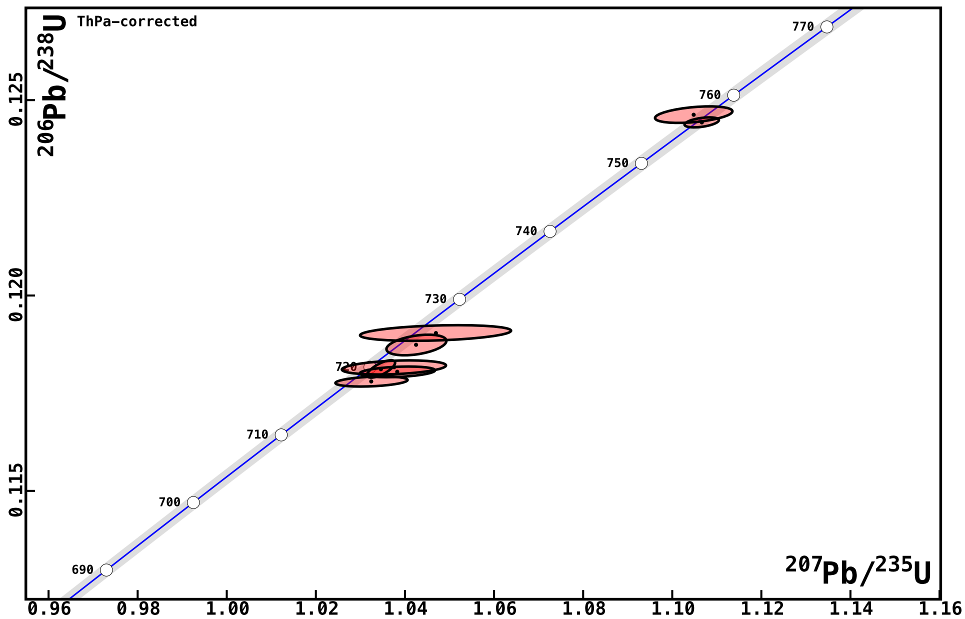

Figure 13. **Concordia diagram for SAM-ET-03 showing all the analyses**

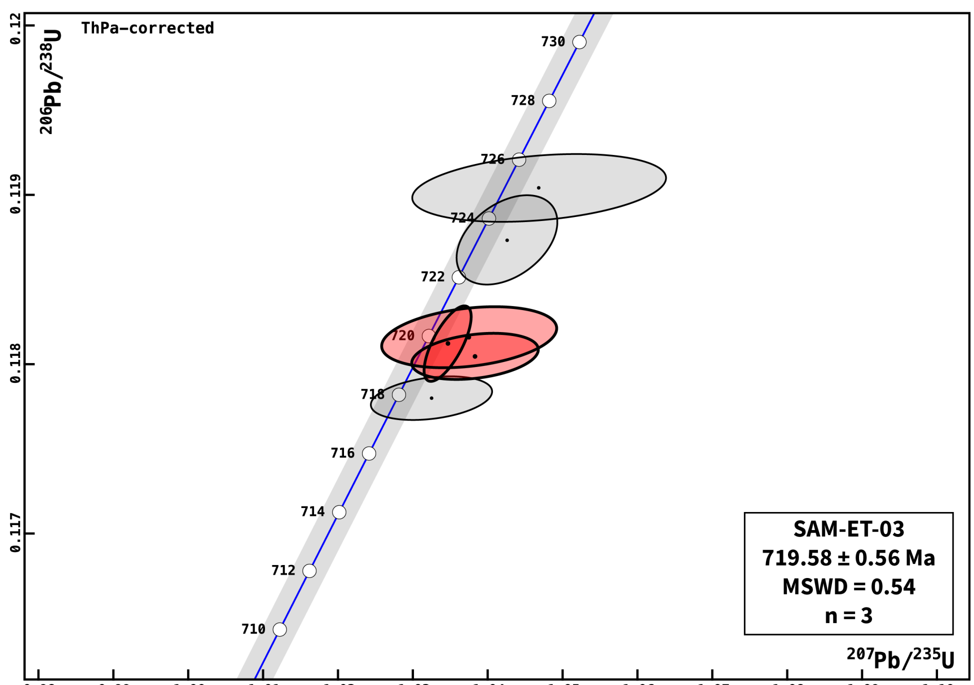

Figure 14. **Zoomed-in concordia diagram for SAM-ET-03. The weighted mean date with associated statistical parameters for the sample is shown (2σ analytical uncertainty).**

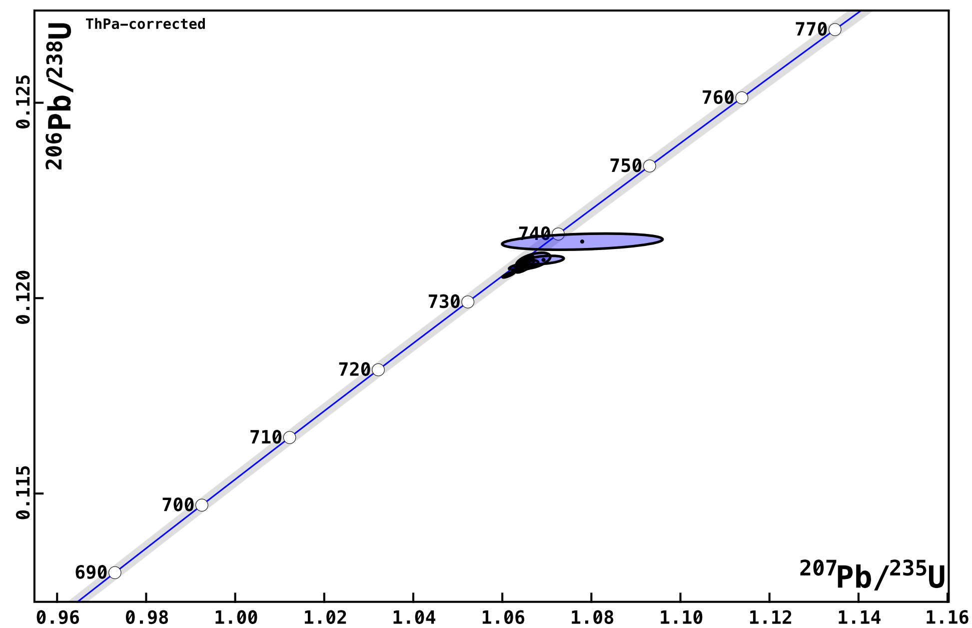

Figure 15. **Concordia diagram for T46-102_2Z showing all the analyses**

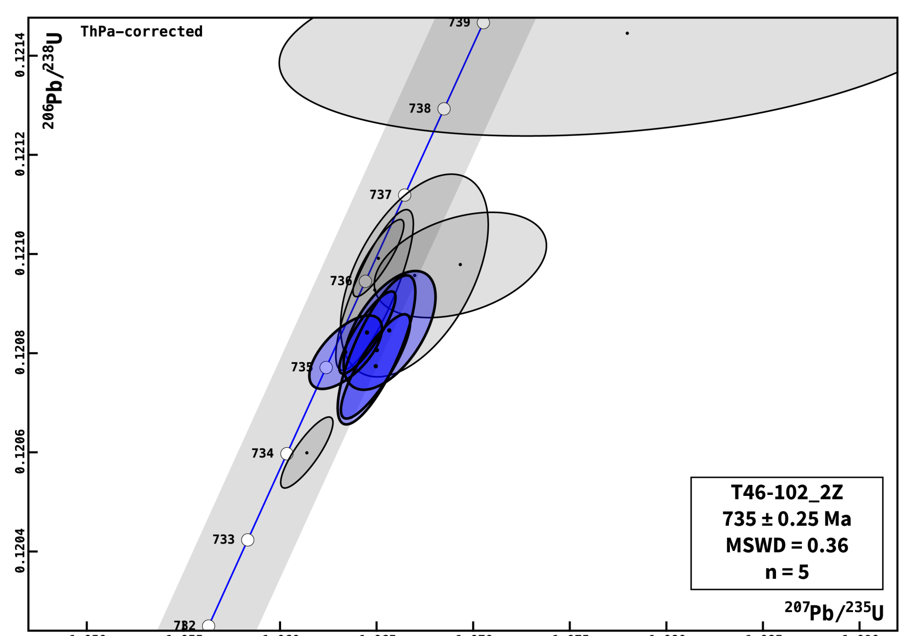

Figure 16. **Concordia diagram for T46-102_2Z. The weighted mean date with associated statistical parameters for the sample is shown (2σ analytical uncertainty).**

Further discussion of interpretation of the geochronological data

Motivation for existing interpretation

In the manuscript, an interpretation is put forward that the two upper samples represent depositional ages based on the coherent population of zircons that overlap within ~1 Ma of each other. In laser ablation studies similar instances are frequently encountered, but the uncertainties are large enough (±15 Ma is typical for Neoproterozoic zircon grains) that coherent populations of zircons may have come from different sources and are therefore probably a detrital signal. In the case of the samples SAM-ET-03 and SAM-ET-04, the uncertainties are small enough (±1 Ma) that a proximal source of uniform age material would be required, such as granitic material with an age of ~719Ma. Granitic material of this or similar ages has not been discovered in the east African portion of the Arabian Nubian Shield, therefore making this an unlikely explanation for the age clusters observed.

Additionally, younger analyses in all three samples have been attributed to incomplete dissolution of regions of zircons that have experience Pb-loss. Pervasive Pb-loss is ubiquitous in Precambrian zircons. Recent ID-TIMS studies have shown similar results of coherent clusters of zircon ages with a small number of isolated analyses that were also attributed to Pb-loss. For example Macdonald et al. (2010) published ages for a rhyolite tuff that exhibited two clusters of zircon ages, one slightly younger than the other. They favored the older cluster of ages as representing the depositional age of the tuff as more intense chemical abrasion at higher temperatures reproduced the older ages. The same behavior was observed in a more recent study by Macdonald et al. (2017), where one sample had a cluster of zircon ages, with isolated younger ages. The younger ages were attributed to Pb-loss as higher temperature chemical abrasion reproduced the older consistent cluster of ages.

Alternative interpretations

Below, alternative interpretations to the U-Pb geochronological data are described. The two samples highest in the stratigraphy, SAM-ET-03 and SAM-ET-04 are dealt with first. If all the zircons are interpreted as being detrital, then the youngest grains in each sample could be interpreted as representing the maximum age, which would be 698 and 717.9 Ma for SAM-ET-04 and SAM-ET-03 respectively. That would mean that all the stratigraphy above SAM-ET-04 would be younger than 698 Ma, and therefore the Negash diamictite above would have no temporal association with the Sturtian glaciation.

Alternatively, the dates younger than ~719 Ma could be interpreted as the result of Pb-loss, but that due to the detrital input in both samples, the cluster of ages at 719 Ma should be interpreted as a maximum depositional age, that is temporally close to its true depositional age. This interpretation would not change substantially change the conclusions of the paper, that is, the Negash diamictite is probably Sturtian in age, the Islay anomaly precedes the glaciation by at least 18 Ma and that δ^{13}C of inorganic carbon as recorded by carbonates remains stable at positive values for the duration between the Islay anomaly and the Sturtian glaciation.

Both SAM-ET-03 and SAM-ET-04 have single analyses with an age of ~718 Ma (see U-Pb data table). The analysis is included in the weighted mean in the case of SAM-ET-04, but is excluded from the SAM-ET-03 weighted mean because it drastically increases the mean square of weighted deviates (MSWD). Another alternative interpretation is that these single analyses with ages of ~718 Ma represent the depositional age. Using ~718 Ma as the deposition age for the SAM-ET-03 and SAM-ET-04 tuffs would change the monte carlo estimate by ~2 Ma to 715.1 Ma. This estimate barely overlaps with the age constraints from Laurentia and would imply either that Sturtian glacial sediments are not globally synchronous, or that the Negash diamictite is not glacial or related the Sturtian Snowball Earth.

Carbon isotope methods

Carbonate samples were cut perpendicular to bedding to expose a fresh surface before micro-drilling. Clearly altered zones of the fresh surface, such as those affected by veining and fractures, were avoided. Carbonate powders were weighed out to 1 mg, then heated to 110 °C to remove any residual water. Samples then were reacted with 250 μL of H_3PO_4 at 75 °C. The resulting CO_2 gas was extracted using a GasBench II auto-sampler and simultaneously analyzed for δ^{13}C and δ^{18}O on a SerCon Callisto continuous-flow isotope ratio mass spectrometry (CF-IRMS) system at Princeton University. NBS-19 (δ^{13}C = 1.95 ‰ and δ^{18}O = -2.20 ‰) and an internally calibrated standard (δ^{13}C = -1.48 ± 0.1 ‰ and δ^{18}O = -8.54 ± 0.1 ‰) also were analyzed once every 10 samples to correct the raw measurements. Measured precision was = 0.1 ‰ for δ^{13}C and σ = 0.2 ‰ for δ^{18}O.

Carbon isotope composite

δ^{13}C data from the Samre Fold-Thrust Belt are developed in this study, and δ^{13}C data from the Negash Syncline are developed in Swanson-Hysell et al. (2015), and are supplemented by this study. Correlations between sections in the the Samre Fold-Thrust Belt and Negash Syncline are made through the correlation of the formation contacts. Since Tambien Group stratigraphy hosts carbonates conformable with Sturtian glacial deposits, and since our new U-Pb ID-TIMS constraints of 735.25 ± 0.25, 719.58 ± 0.56, and 719.68 ± 0.46 Ma from this study place tight constraints on the timing of the Islay Anomaly and the onset of the Sturtian Glaciation in Ethiopia, we use the Tambien Group δ^{13}C curve as the backbone for making correlations with other datasets. With the notable exception of 732.2 ± 4.7 (Rooney et al., 2014) and 739.9 ± 6.1 Ma (Strauss et al., 2014) Re-Os isochrons from Canada, no direct age constraints exist on δ^{13}C data between 745 and 717 Ma from any of the basins included in this composite. We therefore correlated the downturn, nadir, and recovery of the Islay Anomaly between these datasets and that of the Tambien Group. While the values of δ^{13}C before the interpreted anomaly are slightly lower in the Tambien Group than other successions, the magnitude of the anomaly is similar across the correlated sections. The age model for pre-Islay anomaly δ^{13}C data was developed on the basis of sedimentation rates inferred from various geochronological, lithological, and chemostratigraphic constraints in each of the basins.

Monte Carlo sedimentation rate estimates

Based on calculations using the mapped formation boundaries and more than 200 measurements of bedding orientation in the Matheos and Mariam Bohkahko Formations together with constraints from measured sections, the stratigraphic thickness between T46-102_2Z (735.25 ± 0.25 Ma) and SAM-ET-03 (719.58 ± 0.56 Ma) was constrained to be between 439 and 538 m. For the Monte Carlo simulation, we randomly picked ages (N=50,000) for the T46-102_2Z and SAM-ET-03 samples from normal distributions about the weighted mean age of each sample, as well as a stratigraphic thickness between the two samples from a uniform distribution between the minimum and maximum values described above. Using these two ages and the stratigraphic thickness, a sedimentation rate was calculated. This rate was then applied to the 85 m of stratigraphy between SAM-ET-03 and the base of the diamictite to estimate the age of the onset of Sturtian Glaciation in the Tambien Group. This same method was applied to the T46-102_2Z and SAM-ET-04 (719.68 ± 0.46 Ma) samples (stratigraphic thickness between the samples constrained to be between 450 and 549 m, and 74 m of stratigraphy between SAM-ET-04 and the base of the diamictite), producing a total of 100,000 Monte Carlo estimates of the age of the onset of Sturtian Glaciation in the Tambien Group shown in Figure 2 of the main text.

Basis for using Linear Sediment Accumulation rates

The facies in the Mariam Bohkahko formation in the western Samre area vary from ribbonite to siltstone with grainstone interbeds and shales(see Fig. 1 in main text). While these changes in facies must indicate variation in sediment accumulation rate or water depth on the short term, there are a several reasons why assuming an average linear sediment accumulation rates is reasonable.

First, the time between the T46-102_Z and SAM-ET-03/04 tuffs is ~15.6 Ma. Short term, facies dependent, sediment accumulation rate changes should be averaged out over this duration. We expect subsidence rate to be the primary control on sediment accumulation rate over these ∼10 Ma timescales. The subsidence rate must have remained relatively constant in this study area as there is little sedimentological evidence for large changes in water depth such as sequence boundaries, unconformities, or deep water deposition.

Second, the approximated age for the contact with the diamictite is ∼2.5 Ma younger than the uppermost tuff (SAM-ET-04). The calculated age difference is extrapolated 16% beyond the total time between age constraints (i.e. 15.6 Ma). We believe the extrapolation is justified given the short duration over which it is applied.

In summary, while it is clear that sediment accumulation rate or water depth must have changed over short time scales as evidence by the facies changes in the Mariam Bohkahko formation in western Samre, it seems reasonable to assume linear sedimentation rates over the million year timescales of interest to this study.

References

Gerstenberger, H. and Haase, G., 1997, A highly effective emitter substance for mass spectrometric Pb isotope ratio determinations: Chemical geology, vol. 136, pp. 309–312.

Knoll, A., Hayes, J., Kaufman, A., Swett, K., and Lambert, I., 1986, Secular variation in carbon isotope ratios from upper proterozoic successions of svalbard and east greenland: Nature, vol. 321, pp. 832–838.

Macdonald, F. A., Schmitz, M. D., Crowley, J. L., Roots, C. F., Jones, D. S., Maloof, A. C., Strauss, J. V., Cohen, P. A., Johnston, D. T., and Schrag, D. P., 2010, Calibrating the Cryogenian: Science, vol. 327, pp. 1241–1243, doi:10.1126/science.1183325.

Macdonald, F. A., Schmitz, M. D., Strauss, J. V., Halverson, G. P., Gibson, T. M., Eyster, A., Cox, G., Mamrol, P., and Crowley, J. L., 2017, Cryogenian of Yukon: Precambrian Research, doi: 10.1016/j.precamres.2017.08.015, URL http://dx.doi.org/10.1016/j.precamres.2017.08.015.

Rooney, A. D., Macdonald, F. A., Strauss, J. V., Dudás, F. Ö., Hallmann, C., and Selby, D., 2014, Re-Os geochronology and coupled Os-Sr isotope constraints on the Sturtian snowball Earth: Proceedings of the National Academy of Sciences, vol. 111, pp. 51–56, doi:10.1073/pnas.1317266110.

Strauss, J. V., Rooney, A. D., Macdonald, F. A., Brandon, A. D., and Knoll, A. H., 2014, 740 Ma vase-shaped microfossils from Yukon, Canada: Implications for Neoproterozoic chronology and biostratigraphy: Geology, doi:10.1130/G35736.1.

Swanson-Hysell, N. L., Maloof, A. C., Condon, D. J., Jenkin, G. R. T., Alene, M., Tremblay, M. M., Tesema, T., Rooney, A. D., and Haileab, B., 2015, Stratigraphy and geochronology of the Tambien Group, Ethiopia: Evidence for globally synchronous carbon isotope change in the Neoproterozoic: Geology, doi: 10.1130/G36347.1.

Upper Tambien Group Geochronology

	Dates (Ma)							Composition				Isotopic Ratios														
Fraction	206Pb/ 238U <Th> a	±2σ abs	207Pb/ 235U <Pa> c	±2σ abs	207Pb/ 206Pb <ThPa> ac	±2σ abs	% disc d	Th/ U e	Pb* (pg) f	Pbc (pg) g	Pb*/ Pbc h	206Pb/ 204Pb i	208Pb/ 206Pb j	206Pb/ 238U <Th> ja	±2σ %	206Pb/ 238U j	±2σ %	207Pb/ 235U <Pa> jc	±2σ %	207Pb/ 235U j	±2σ %	207Pb/ 206Pb <ThPa> jac	±2σ %	207Pb/ 206Pb j	±2σ %	Corr. coef.
SAM-ET-03	**N 13.13976 S 39.17616 (Decimal degrees WGS 84)**																									
z7	717.89	0.74	720.17	4.05	727.30	16.08	1.35	0.29	12.48	0.68	18.30	1165.33	0.09	0.12	0.11	0.12	0.11	1.03	0.78	1.03	0.78	0.06	0.76	0.06	0.76	0.30
z2	719.31	0.78	723.07	4.21	734.77	16.69	2.16	0.18	8.03	0.46	17.41	1140.81	0.06	0.12	0.12	0.12	0.12	1.04	0.81	1.04	0.81	0.06	0.79	0.06	0.79	0.29
z23	719.74	1.28	721.25	1.57	725.94	4.55	0.90	0.31	12.86	0.17	77.04	4821.88	0.09	0.12	0.19	0.12	0.19	1.03	0.30	1.03	0.30	0.06	0.21	0.06	0.21	0.71
z4	719.96	1.04	722.69	5.82	731.15	23.13	1.58	0.34	6.23	0.48	12.89	813.52	0.11	0.12	0.15	0.12	0.15	1.04	1.13	1.04	1.13	0.06	1.09	0.06	1.09	0.29
z22	723.27	1.52	725.20	3.34	731.16	12.56	1.13	0.30	4.88	0.17	28.68	1811.07	0.09	0.12	0.22	0.12	0.22	1.04	0.65	1.04	0.65	0.06	0.59	0.06	0.59	0.40
z3	725.04	1.15	727.33	8.41	734.40	33.41	1.32	0.29	8.42	0.98	8.56	553.67	0.09	0.12	0.17	0.12	0.17	1.05	1.62	1.05	1.62	0.06	1.58	0.06	1.58	0.29
z6	756.01	0.73	756.55	1.86	758.12	6.67	0.32	0.41	18.05	0.39	45.83	2800.89	0.12	0.12	0.10	0.12	0.10	1.11	0.35	1.11	0.35	0.06	0.31	0.06	0.31	0.45
z11	757.15	1.21	755.68	4.19	751.34	15.50	-0.73	0.29	7.18	0.36	20.13	1276.85	0.09	0.12	0.17	0.12	0.17	1.10	0.79	1.10	0.79	0.06	0.73	0.06	0.73	0.41
z5	778.15	0.54	778.06	1.55	777.80	5.43	0.00	0.34	22.34	0.40	55.53	3447.63	0.10	0.13	0.07	0.13	0.07	1.15	0.29	1.15	0.29	0.07	0.26	0.07	0.26	0.48
z13	800.11	1.53	805.85	6.07	821.76	21.78	2.67	0.52	5.40	0.39	13.82	833.06	0.16	0.13	0.20	0.13	0.20	1.21	1.09	1.21	1.09	0.07	1.04	0.07	1.04	0.32
z8	801.31	1.59	798.29	11.36	789.84	41.91	-1.41	0.34	5.27	0.77	6.85	441.03	0.10	0.13	0.21	0.13	0.21	1.20	2.06	1.20	2.06	0.07	2.00	0.07	2.00	0.32
SAM-ET-04	**N 13.13980 S 39.17630 (Decimal degrees WGS 84)**																									
z3	698.17	1.06	702.93	7.54	718.18	30.76	2.84	0.25	4.76	0.50	9.43	615.32	0.08	0.11	0.16	0.11	0.16	1.00	1.49	1.00	1.49	0.06	1.45	0.06	1.45	0.28
z28	713.52	1.52	713.36	8.49	712.83	34.25	-0.05	0.32	11.08	1.22	9.05	580.39	0.10	0.12	0.23	0.12	0.23	1.02	1.66	1.02	1.66	0.06	1.61	0.06	1.61	0.27
z33	717.99	1.43	717.29	5.34	715.11	21.03	-0.35	0.28	9.93	0.68	14.54	932.70	0.09	0.12	0.21	0.12	0.21	1.03	1.04	1.03	1.04	0.06	0.99	0.06	0.99	0.32
z2	718.90	2.41	720.53	19.52	725.63	78.44	0.98	0.31	14.65	3.98	3.68	247.44	0.10	0.12	0.35	0.12	0.35	1.03	3.78	1.03	3.78	0.06	3.70	0.06	3.70	0.28
z16	719.41	1.20	724.40	9.23	739.87	36.84	2.81	0.31	10.57	1.36	7.75	501.19	0.09	0.12	0.18	0.12	0.18	1.04	1.78	1.04	1.78	0.06	1.74	0.06	1.74	0.28
z12	719.80	0.83	719.15	5.90	717.13	23.71	-0.32	0.30	14.34	1.17	12.23	782.55	0.09	0.12	0.12	0.12	0.12	1.03	1.14	1.03	1.14	0.06	1.12	0.06	1.12	0.28
z39	719.80	2.21	722.96	4.37	732.77	16.22	1.82	0.27	5.54	0.26	20.99	1339.32	0.08	0.12	0.32	0.12	0.32	1.04	0.84	1.04	0.84	0.06	0.76	0.06	0.76	0.42
z41	719.92	1.57	724.78	7.58	739.85	29.88	2.74	0.37	2.93	0.27	10.90	686.46	0.11	0.12	0.23	0.12	0.23	1.04	1.46	1.04	1.46	0.06	1.41	0.06	1.41	0.29
z38	719.98	1.23	723.10	8.13	732.77	32.39	1.79	0.35	5.99	0.64	9.34	594.25	0.11	0.12	0.18	0.12	0.18	1.04	1.57	1.04	1.57	0.06	1.53	0.06	1.53	0.29
z11	720.65	1.20	723.95	8.48	734.19	33.84	1.89	0.41	5.96	0.68	8.78	551.11	0.13	0.12	0.18	0.12	0.18	1.04	1.64	1.04	1.64	0.06	1.60	0.06	1.60	0.28
z37	721.61	5.19	725.13	6.94	736.01	22.85	2.01	0.31	7.19	0.54	13.29	846.92	0.09	0.12	0.76	0.12	0.76	1.04	1.34	1.04	1.34	0.06	1.08	0.06	1.08	0.59
z43	722.01	1.36	724.14	3.62	730.77	13.69	1.24	0.51	5.29	0.21	25.68	1537.30	0.16	0.12	0.20	0.12	0.20	1.04	0.70	1.04	0.70	0.06	0.65	0.06	0.65	0.40
z13	728.00	3.07	737.02	23.84	764.55	93.62	4.83	0.35	5.99	1.95	3.08	207.55	0.11	0.12	0.45	0.12	0.45	1.07	4.55	1.07	4.55	0.06	4.44	0.06	4.44	0.29
z40	731.11	1.26	734.30	5.74	744.04	22.50	1.78	0.60	3.15	0.21	15.03	886.34	0.19	0.12	0.18	0.12	0.18	1.06	1.10	1.06	1.10	0.06	1.06	0.06	1.06	0.27
z7	745.51	2.63	752.64	17.06	773.90	65.69	3.71	0.37	1.70	0.38	4.42	289.08	0.11	0.12	0.37	0.12	0.37	1.10	3.21	1.10	3.21	0.07	3.12	0.07	3.12	0.29
z30	764.10	4.54	761.32	29.96	753.17	114.95	-1.41	0.33	0.90	0.36	2.53	174.77	0.10	0.13	0.63	0.13	0.63	1.12	5.59	1.12	5.59	0.06	5.44	0.06	5.44	0.29
z24	776.19	0.89	775.96	3.06	775.29	11.22	-0.08	0.52	7.80	0.27	28.96	1723.12	0.16	0.13	0.12	0.13	0.12	1.15	0.56	1.15	0.56	0.07	0.53	0.07	0.53	0.35
z15	785.03	1.75	786.26	5.45	789.76	19.86	0.64	0.40	21.01	1.45	14.51	900.19	0.12	0.13	0.24	0.13	0.24	1.17	1.00	1.17	1.00	0.07	0.95	0.07	0.95	0.32
z36	789.88	4.29	792.25	7.19	798.92	24.51	1.17	0.48	5.13	0.39	13.05	793.77	0.15	0.13	0.58	0.13	0.58	1.18	1.31	1.18	1.31	0.07	1.17	0.07	1.17	0.45
z6	792.67	2.03	795.97	11.71	805.21	43.17	1.60	0.12	3.98	0.65	6.16	421.55	0.04	0.13	0.27	0.13	0.27	1.19	2.12	1.19	2.12	0.07	2.06	0.07	2.06	0.28
z27	801.91	2.33	806.64	8.64	819.73	31.14	2.21	0.33	4.40	0.47	9.34	595.56	0.10	0.13	0.31	0.13	0.31	1.21	1.55	1.21	1.55	0.07	1.49	0.07	1.49	0.29
z9	806.14	0.79	805.69	5.52	804.45	20.31	-0.17	0.46	11.21	0.79	14.15	863.92	0.14	0.13	0.10	0.13	0.10	1.21	0.99	1.21	0.99	0.07	0.97	0.07	0.97	0.27
z17	814.16	3.15	826.23	22.56	858.85	80.73	5.24	0.51	4.47	1.28	3.49	224.14	0.16	0.13	0.41	0.13	0.41	1.26	3.99	1.26	3.99	0.07	3.89	0.07	3.89	0.29
z35	820.81	7.67	834.26	19.94	870.26	68.22	5.72	0.39	2.81	0.67	4.18	272.40	0.12	0.14	1.00	0.14	1.00	1.27	3.51	1.27	3.51	0.07	3.29	0.07	3.29	0.35
z10	824.53	3.78	839.36	28.33	878.81	100.28	6.21	0.34	5.03	1.92	2.62	179.62	0.10	0.14	0.49	0.14	0.49	1.29	4.96	1.29	4.96	0.07	4.85	0.07	4.85	0.28
z4	833.92	1.07	837.01	5.57	845.20	19.71	1.37	0.39	5.94	0.41	14.42	895.56	0.12	0.14	0.14	0.14	0.14	1.28	0.98	1.28	0.98	0.07	0.95	0.07	0.95	0.28
z14	844.49	22.89	930.57	159.22	1140.43	506.47	25.97	0.77	1.61	3.29	0.49	45.11	0.24	0.14	2.89	0.14	2.89	1.50	26.13	1.50	26.13	0.08	25.47	0.08	25.47	0.28
z8	845.46	1.42	848.91	9.99	857.96	35.23	1.49	0.50	8.27	1.04	7.97	489.60	0.15	0.14	0.18	0.14	0.18	1.31	1.74	1.31	1.74	0.07	1.70	0.07	1.70	0.27
z20	864.97	1.07	864.98	5.99	865.00	20.67	0.04	0.32	9.48	0.72	13.14	832.47	0.10	0.14	0.13	0.14	0.13	1.34	1.03	1.34	1.03	0.07	1.00	0.07	1.00	0.30
T46-102_2Z	**N 13.15873 S 39.25126 (Decimal degrees WGS 84)**																									
z18	734.01	0.41	734.51	0.67	736.01	1.77	0.32	0.46	219.74	0.83	263.49	15786.41	0.14	0.12	0.06	0.12	0.06	1.06	0.13	1.06	0.13	0.06	0.08	0.06	0.08	0.84
z20	735.01	0.60	736.26	0.88	740.05	2.26	0.73	0.26	40.38	0.24	167.39	10579.88	0.08	0.12	0.09	0.12	0.09	1.06	0.17	1.06	0.17	0.06	0.10	0.06	0.10	0.84
z19	735.18	0.43	735.50	0.93	736.47	3.07	0.23	0.26	65.86	0.63	104.15	6595.40	0.08	0.12	0.06	0.12	0.06	1.06	0.18	1.06	0.18	0.06	0.14	0.06	0.14	0.64
z15	735.20	0.86	736.28	0.99	739.56	2.56	0.64	0.26	35.04	0.22	159.80	10104.90	0.08	0.12	0.12	0.12	0.12	1.06	0.19	1.07	0.19	0.06	0.12	0.06	0.12	0.78
z25	735.41	0.48	736.05	0.71	738.02	1.80	0.40	0.39	113.45	0.35	325.28	19866.97	0.12	0.12	0.07	0.12	0.07	1.06	0.14	1.06	0.14	0.06	0.08	0.06	0.08	0.86
z17	735.43	0.69	736.62	1.17	740.22	3.94	0.70	0.22	21.25	0.25	84.24	5390.98	0.07	0.12	0.10	0.12	0.10	1.07	0.22	1.07	0.22	0.06	0.18	0.06	0.18	0.56
z12	735.90	0.93	736.23	0.99	737.25	2.32	0.23	0.26	36.59	0.18	199.17	12591.49	0.08	0.12	0.13	0.12	0.13	1.06	0.19	1.06	0.19	0.06	0.10	0.06	0.10	0.82
z22	736.07	1.18	737.25	1.88	740.83	6.56	0.69	0.28	26.39	0.59	44.63	2823.63	0.08	0.12	0.17	0.12	0.17	1.07	0.36	1.07	0.36	0.06	0.31	0.06	0.31	0.50
z23	736.19	0.61	738.42	2.19	745.17	8.31	1.25	0.29	17.90	0.50	36.14	2280.85	0.09	0.12	0.09	0.12	0.09	1.07	0.42	1.07	0.42	0.06	0.39	0.06	0.39	0.37
z21	736.27	0.45	736.33	0.65	736.52	1.61	0.08	0.20	105.91	0.29	369.31	23728.05	0.06	0.12	0.06	0.12	0.06	1.07	0.12	1.07	0.12	0.06	0.07	0.06	0.07	0.86
z24	738.88	1.19	742.65	8.80	754.03	34.41	2.06	0.26	7.23	0.89	8.12	531.25	0.08	0.12	0.17	0.12	0.17	1.08	1.67	1.08	1.67	0.06	1.63	0.06	1.63	0.29

Highlighted cells were used for weighted mean calculations

a Corrected for initial Th/U disequilibrium using radiogenic 208Pb and Th/U[magma] = 2.80000.
b Isotopic dates calculated using λ238 = 1.55125E-10 (Jaffey et al. 1971) and λ235 = 9.8485E-10 (Jaffey et al. 1971).
c Corrected for initial Pa/U disequilibrium using initial fraction activity ratio [231Pa]/[235U] = 1.10000.
d % discordance = 100 - (100 * (206Pb/238U date) / (207Pb/206Pb date))
e Th contents calculated from radiogenic 208Pb and 230Th-corrected 206Pb/238U date of the sample, assuming concordance between U-Pb Th-Pb systems.
f Total mass of radiogenic Pb.
g Total mass of common Pb.
h Ratio of radiogenic Pb (including 208Pb) to common Pb.
i Measured ratio corrected for fractionation and spike contribution only.
j Measured ratios corrected for fractionation, tracer and blank.

Field area	Source	Section	stratigraphic height (m)	Model age (Ma)	d13C
Negash Syncline	Swanson-Hysell et al. (2015); this study	T22	3285.3	744.94	2.52
Negash Syncline	Swanson-Hysell et al. (2015); this study	T22	3301.3	744.68	2.21
Negash Syncline	Swanson-Hysell et al. (2015); this study	T22	3326.8	744.26	2.87
Negash Syncline	Swanson-Hysell et al. (2015); this study	T22	3337.7	744.08	2.41
Negash Syncline	Swanson-Hysell et al. (2015); this study	T22	3368.6	743.56	2.31
Negash Syncline	Swanson-Hysell et al. (2015); this study	T22	3383.6	743.32	2.06
Negash Syncline	Swanson-Hysell et al. (2015); this study	T22	3395.8	743.11	1.91
Negash Syncline	Swanson-Hysell et al. (2015); this study	T22	3401.5	743.02	1.7
Negash Syncline	Swanson-Hysell et al. (2015); this study	T22	3412.7	742.83	2.48
Negash Syncline	Swanson-Hysell et al. (2015); this study	T22	3420.3	742.71	2.11
Negash Syncline	Swanson-Hysell et al. (2015); this study	T22	3430.1	742.55	2.48
Negash Syncline	Swanson-Hysell et al. (2015); this study	T22	3438.2	742.41	2.95
Negash Syncline	Swanson-Hysell et al. (2015); this study	T22	3445.9	742.28	2.61
Negash Syncline	Swanson-Hysell et al. (2015); this study	T22	3462.4	742.01	2.73
Negash Syncline	Swanson-Hysell et al. (2015); this study	T22	3477.6	741.76	2.52
Negash Syncline	Swanson-Hysell et al. (2015); this study	T22	3569	740.25	2.73
Negash Syncline	Swanson-Hysell et al. (2015); this study	T22	3621.4	739.38	-0.02
Negash Syncline	Swanson-Hysell et al. (2015); this study	T23	3310.3	744.53	2.47
Negash Syncline	Swanson-Hysell et al. (2015); this study	T23	3314.3	744.46	1.8
Negash Syncline	Swanson-Hysell et al. (2015); this study	T23	3316.2	744.43	1.33
Negash Syncline	Swanson-Hysell et al. (2015); this study	T23	3319	744.39	2.41
Negash Syncline	Swanson-Hysell et al. (2015); this study	T23	3322.9	744.32	2.19
Negash Syncline	Swanson-Hysell et al. (2015); this study	T23	3325.8	744.27	2.19
Negash Syncline	Swanson-Hysell et al. (2015); this study	T23	3328.8	744.22	2.77
Negash Syncline	Swanson-Hysell et al. (2015); this study	T23	3335.1	744.12	1.58
Negash Syncline	Swanson-Hysell et al. (2015); this study	T23	3340.2	744.03	1.27
Negash Syncline	Swanson-Hysell et al. (2015); this study	T23	3341.7	744.01	1.56
Negash Syncline	Swanson-Hysell et al. (2015); this study	T23	3344.7	743.96	1.57
Negash Syncline	Swanson-Hysell et al. (2015); this study	T23	3347.8	743.91	1.74
Negash Syncline	Swanson-Hysell et al. (2015); this study	T23	3349.7	743.88	1.59
Negash Syncline	Swanson-Hysell et al. (2015); this study	T23	3353.4	743.82	2.2
Negash Syncline	Swanson-Hysell et al. (2015); this study	T23	3354.5	743.8	2.04
Negash Syncline	Swanson-Hysell et al. (2015); this study	T23	3357.3	743.75	1.6
Negash Syncline	Swanson-Hysell et al. (2015); this study	T23	3359.5	743.72	2.29
Negash Syncline	Swanson-Hysell et al. (2015); this study	T23	3361.5	743.68	2
Negash Syncline	Swanson-Hysell et al. (2015); this study	T23	3363.3	743.65	1.55
Negash Syncline	Swanson-Hysell et al. (2015); this study	T23	3364.4	743.63	1.81
Negash Syncline	Swanson-Hysell et al. (2015); this study	T23	3370.1	743.54	0.55
Negash Syncline	Swanson-Hysell et al. (2015); this study	T23	3372.2	743.51	1.97
Negash Syncline	Swanson-Hysell et al. (2015); this study	T23	3382	743.34	2.6
Negash Syncline	Swanson-Hysell et al. (2015); this study	T23	3385.5	743.28	2
Negash Syncline	Swanson-Hysell et al. (2015); this study	T23	3387.5	743.25	2.86
Negash Syncline	Swanson-Hysell et al. (2015); this study	T23	3389.7	743.22	1.41
Negash Syncline	Swanson-Hysell et al. (2015); this study	T23	3391.7	743.18	2.22
Negash Syncline	Swanson-Hysell et al. (2015); this study	T23	3392.9	743.16	2.6
Negash Syncline	Swanson-Hysell et al. (2015); this study	T23	3409.4	742.89	3.28
Negash Syncline	Swanson-Hysell et al. (2015); this study	T23	3415.9	742.78	2.25
Negash Syncline	Swanson-Hysell et al. (2015); this study	T23	3422.9	742.67	2.64
Negash Syncline	Swanson-Hysell et al. (2015); this study	T23	3426.7	742.6	1.87
Negash Syncline	Swanson-Hysell et al. (2015); this study	T23	3429.2	742.56	2.58
Negash Syncline	Swanson-Hysell et al. (2015); this study	T23	3433.4	742.49	2.54
Negash Syncline	Swanson-Hysell et al. (2015); this study	T23	3435.5	742.46	2.89
Negash Syncline	Swanson-Hysell et al. (2015); this study	T23	3452.5	742.18	2.22
Negash Syncline	Swanson-Hysell et al. (2015); this study	T23	3454.9	742.14	2.74
Negash Syncline	Swanson-Hysell et al. (2015); this study	T23	3462.2	742.01	2.53
Negash Syncline	Swanson-Hysell et al. (2015); this study	T23	3469.3	741.9	1.97
Negash Syncline	Swanson-Hysell et al. (2015); this study	T23	3476.4	741.78	2.3
Negash Syncline	Swanson-Hysell et al. (2015); this study	T23	3478.7	741.74	2.34
Negash Syncline	Swanson-Hysell et al. (2015); this study	T23	3481.8	741.69	2.66

Negash Syncline	Swanson-Hysell et al. (2015); this study	T23	3501.5	741.36	2.42
Negash Syncline	Swanson-Hysell et al. (2015); this study	T23	3504.3	741.32	2.15
Negash Syncline	Swanson-Hysell et al. (2015); this study	T23	3509.5	741.23	3.08
Negash Syncline	Swanson-Hysell et al. (2015); this study	T23	3513	741.17	2.88
Negash Syncline	Swanson-Hysell et al. (2015); this study	T23	3519.5	741.07	3.14
Negash Syncline	Swanson-Hysell et al. (2015); this study	T23	3522.1	741.02	2.75
Negash Syncline	Swanson-Hysell et al. (2015); this study	T23	3525.6	740.96	3.33
Negash Syncline	Swanson-Hysell et al. (2015); this study	T23	3530.4	740.89	2.8
Negash Syncline	Swanson-Hysell et al. (2015); this study	T23	3532.2	740.86	2.92
Negash Syncline	Swanson-Hysell et al. (2015); this study	T23	3540.6	740.72	2.62
Negash Syncline	Swanson-Hysell et al. (2015); this study	T23	3543.4	740.67	2.44
Negash Syncline	Swanson-Hysell et al. (2015); this study	T23	3547.3	740.61	2.33
Negash Syncline	Swanson-Hysell et al. (2015); this study	T23	3552.3	740.52	2.56
Negash Syncline	Swanson-Hysell et al. (2015); this study	T23	3554.8	740.48	2.3
Negash Syncline	Swanson-Hysell et al. (2015); this study	T23	3558.6	740.42	3.22
Negash Syncline	Swanson-Hysell et al. (2015); this study	T23	3560.3	740.39	3.63
Negash Syncline	Swanson-Hysell et al. (2015); this study	T23	3578.9	740.08	3.39
Negash Syncline	Swanson-Hysell et al. (2015); this study	T23	3583.2	740.01	3.28
Negash Syncline	Swanson-Hysell et al. (2015); this study	T23	3585.3	739.98	2.98
Negash Syncline	Swanson-Hysell et al. (2015); this study	T23	3590.6	739.89	2.55
Negash Syncline	Swanson-Hysell et al. (2015); this study	T23	3592.9	739.85	2.84
Negash Syncline	Swanson-Hysell et al. (2015); this study	T23	3596.1	739.8	3.26
Negash Syncline	Swanson-Hysell et al. (2015); this study	T23	3600.9	739.72	4.41
Negash Syncline	Swanson-Hysell et al. (2015); this study	T23	3602	739.7	3.94
Negash Syncline	Swanson-Hysell et al. (2015); this study	T23	3605.6	739.64	3.68
Negash Syncline	Swanson-Hysell et al. (2015); this study	T23	3607.5	739.61	3.99
Negash Syncline	Swanson-Hysell et al. (2015); this study	T23	3612.4	739.53	3.14
Negash Syncline	Swanson-Hysell et al. (2015); this study	T23	3615.2	739.48	2.3
Negash Syncline	Swanson-Hysell et al. (2015); this study	T23	3617.2	739.45	2.37
Negash Syncline	Swanson-Hysell et al. (2015); this study	T23	3619.4	739.41	2.28
Negash Syncline	Swanson-Hysell et al. (2015); this study	T23	3620.9	739.39	1.91
Negash Syncline	Swanson-Hysell et al. (2015); this study	T23	3623.3	739.35	2.23
Negash Syncline	Swanson-Hysell et al. (2015); this study	T23	3651.6	738.88	1.07
Negash Syncline	Swanson-Hysell et al. (2015); this study	T23	3661.4	738.72	1.14
Negash Syncline	Swanson-Hysell et al. (2015); this study	T23	3664.5	738.66	0.09
Negash Syncline	Swanson-Hysell et al. (2015); this study	T23	3672.3	738.54	0.22
Negash Syncline	Swanson-Hysell et al. (2015); this study	T23	3673.2	738.52	-0.89
Negash Syncline	Swanson-Hysell et al. (2015); this study	T23	3692.4	738.2	-1.36
Negash Syncline	Swanson-Hysell et al. (2015); this study	T23	3700.4	738.07	0.74
Negash Syncline	Swanson-Hysell et al. (2015); this study	T23	3705.2	737.99	-0.21
Negash Syncline	Swanson-Hysell et al. (2015); this study	T23	3708.8	737.93	0.93
Negash Syncline	Swanson-Hysell et al. (2015); this study	T23	3719.4	737.76	1.45
Negash Syncline	Swanson-Hysell et al. (2015); this study	T23	3721.6	737.72	0.95
Negash Syncline	Swanson-Hysell et al. (2015); this study	T23	3722.4	737.71	0.78
Negash Syncline	Swanson-Hysell et al. (2015); this study	T23	3725.3	737.66	-0.08
Negash Syncline	Swanson-Hysell et al. (2015); this study	T23	3732.4	737.54	-0.36
Negash Syncline	Swanson-Hysell et al. (2015); this study	T23	3736.8	737.47	0.43
Negash Syncline	Swanson-Hysell et al. (2015); this study	T23	3746.9	737.3	-1.86
Negash Syncline	Swanson-Hysell et al. (2015); this study	T23	3748.5	737.27	-0.68
Negash Syncline	Swanson-Hysell et al. (2015); this study	T23	3750.8	737.24	-0.19
Negash Syncline	Swanson-Hysell et al. (2015); this study	T23	3752.8	737.2	0.31
Negash Syncline	Swanson-Hysell et al. (2015); this study	T23	3753.2	737.2	-1.26
Negash Syncline	Swanson-Hysell et al. (2015); this study	T23	3764.4	737.01	-4.47
Negash Syncline	Swanson-Hysell et al. (2015); this study	T23	3765.8	736.99	-1.81
Negash Syncline	Swanson-Hysell et al. (2015); this study	T23	3768.4	736.94	-1.48
Negash Syncline	Swanson-Hysell et al. (2015); this study	T23	3800.7	735.9	-11.12
Negash Syncline	Swanson-Hysell et al. (2015); this study	T23	3802	735.66	-10.81
Negash Syncline	Swanson-Hysell et al. (2015); this study	T23	3803.4	735.39	-5.99
Negash Syncline	Swanson-Hysell et al. (2015); this study	T23	3824.1	734.71	5.18
Negash Syncline	Swanson-Hysell et al. (2015); this study	T23	3826.1	734.65	3.7

Negash Syncline	Swanson-Hysell et al. (2015); this study	T23	3828	734.6	3.33
Negash Syncline	Swanson-Hysell et al. (2015); this study	T23	3830.5	734.52	4.52
Negash Syncline	Swanson-Hysell et al. (2015); this study	T23	3833.6	734.43	5.05
Negash Syncline	Swanson-Hysell et al. (2015); this study	T23	3836.1	734.36	6.22
Negash Syncline	Swanson-Hysell et al. (2015); this study	T23	3836.4	734.35	4.51
Negash Syncline	Swanson-Hysell et al. (2015); this study	T23	3837.8	734.31	6.14
Negash Syncline	Swanson-Hysell et al. (2015); this study	T23	3840.3	734.24	5.31
Negash Syncline	Swanson-Hysell et al. (2015); this study	T23	3843.4	734.15	5.51
Negash Syncline	Swanson-Hysell et al. (2015); this study	T23	3845.9	734.08	5.73
Negash Syncline	Swanson-Hysell et al. (2015); this study	T23	3849	733.99	4.23
Negash Syncline	Swanson-Hysell et al. (2015); this study	T23	3852.3	733.89	5.16
Negash Syncline	Swanson-Hysell et al. (2015); this study	T23	3854.2	733.83	5.52
Negash Syncline	Swanson-Hysell et al. (2015); this study	T23	3854.7	733.82	5.4
Negash Syncline	Swanson-Hysell et al. (2015); this study	T23	3856.5	733.77	5.85
Negash Syncline	Swanson-Hysell et al. (2015); this study	T23	3859.7	733.67	5.01
Negash Syncline	Swanson-Hysell et al. (2015); this study	T23	3861.6	733.62	6.17
Negash Syncline	Swanson-Hysell et al. (2015); this study	T23	3864.8	733.53	4.43
Negash Syncline	Swanson-Hysell et al. (2015); this study	T23	3867.5	733.45	6.22
Negash Syncline	Swanson-Hysell et al. (2015); this study	T23	3869.2	733.4	5.89
Negash Syncline	Swanson-Hysell et al. (2015); this study	T23	3871.6	733.33	6.03
Negash Syncline	Swanson-Hysell et al. (2015); this study	T23	3873.6	733.27	3.96
Negash Syncline	Swanson-Hysell et al. (2015); this study	T23	3879.1	733.11	6.08
Negash Syncline	Swanson-Hysell et al. (2015); this study	T23	3882	733.02	4.47
Negash Syncline	Swanson-Hysell et al. (2015); this study	T23	3884	732.97	5.8
Negash Syncline	Swanson-Hysell et al. (2015); this study	T23	3886.6	732.89	5.43
Negash Syncline	Swanson-Hysell et al. (2015); this study	T23	3889.1	732.82	4.29
Negash Syncline	Swanson-Hysell et al. (2015); this study	T23	3890.6	732.77	5.79
Negash Syncline	Swanson-Hysell et al. (2015); this study	T23	3893	732.7	6.95
Negash Syncline	Swanson-Hysell et al. (2015); this study	T23	3894.4	732.66	5.53
Negash Syncline	Swanson-Hysell et al. (2015); this study	T23	3896.4	732.6	6.22
Negash Syncline	Swanson-Hysell et al. (2015); this study	T23	3896.9	732.59	5.81
Negash Syncline	Swanson-Hysell et al. (2015); this study	T23	3899	732.53	4.94
Negash Syncline	Swanson-Hysell et al. (2015); this study	T23	3902	732.44	4.87
Negash Syncline	Swanson-Hysell et al. (2015); this study	T23	3903.9	732.39	5.45
Negash Syncline	Swanson-Hysell et al. (2015); this study	T23	3906	732.32	4.56
Negash Syncline	Swanson-Hysell et al. (2015); this study	T23	3910.1	732.21	5.39
Negash Syncline	Swanson-Hysell et al. (2015); this study	T23	3911.3	732.17	4.75
Negash Syncline	Swanson-Hysell et al. (2015); this study	T23	3913.1	732.12	4.78
Negash Syncline	Swanson-Hysell et al. (2015); this study	T23	3915.2	732.06	4.44
Negash Syncline	Swanson-Hysell et al. (2015); this study	T23	3917.9	731.98	6.22
Negash Syncline	Swanson-Hysell et al. (2015); this study	T23	3919	731.95	6.04
Negash Syncline	Swanson-Hysell et al. (2015); this study	T23	3921.6	731.87	5.03
Negash Syncline	Swanson-Hysell et al. (2015); this study	T23	3924.9	731.77	5.39
Negash Syncline	Swanson-Hysell et al. (2015); this study	T23	3926.3	731.73	4.12
Negash Syncline	Swanson-Hysell et al. (2015); this study	T23	3926.6	731.72	4.1
Negash Syncline	Swanson-Hysell et al. (2015); this study	T23	3930	731.63	5.81
Negash Syncline	Swanson-Hysell et al. (2015); this study	T23	3932.9	731.54	5.21
Negash Syncline	Swanson-Hysell et al. (2015); this study	T23	3935.5	731.47	5.69
Negash Syncline	Swanson-Hysell et al. (2015); this study	T23	3936.7	731.43	4.71
Negash Syncline	Swanson-Hysell et al. (2015); this study	T23	3939.4	731.35	4.96
Negash Syncline	Swanson-Hysell et al. (2015); this study	T23	3941.7	731.28	5.8
Negash Syncline	Swanson-Hysell et al. (2015); this study	T23	3945.3	731.18	6.08
Negash Syncline	Swanson-Hysell et al. (2015); this study	T23	3947.4	731.12	5.29
Negash Syncline	Swanson-Hysell et al. (2015); this study	T23	3948.7	731.08	6.27
Negash Syncline	Swanson-Hysell et al. (2015); this study	T23	3951.3	731	5.49
Negash Syncline	Swanson-Hysell et al. (2015); this study	T23	3953.4	730.94	6.1
Negash Syncline	Swanson-Hysell et al. (2015); this study	T23	3955.2	730.89	5.99
Negash Syncline	Swanson-Hysell et al. (2015); this study	T23	3957.8	730.82	4.48
Negash Syncline	Swanson-Hysell et al. (2015); this study	T23	3963.4	730.65	5.12
Negash Syncline	Swanson-Hysell et al. (2015); this study	T23	3966.8	730.55	5.11

Negash Syncline	Swanson-Hysell et al. (2015); this study	T23	3968.8	730.49	6.21
Negash Syncline	Swanson-Hysell et al. (2015); this study	T23	3969.8	730.47	5.93
Negash Syncline	Swanson-Hysell et al. (2015); this study	T23	3970.5	730.45	5.36
Negash Syncline	Swanson-Hysell et al. (2015); this study	T23	3972.4	730.39	6.08
Negash Syncline	Swanson-Hysell et al. (2015); this study	T23	3973.1	730.37	6.36
Negash Syncline	Swanson-Hysell et al. (2015); this study	T23	3977.3	730.25	6.52
Negash Syncline	Swanson-Hysell et al. (2015); this study	T23	3981	730.14	6.3
Negash Syncline	Swanson-Hysell et al. (2015); this study	T23	3982.5	730.1	5.73
Negash Syncline	Swanson-Hysell et al. (2015); this study	T23	3984.4	730.04	5.35
Negash Syncline	Swanson-Hysell et al. (2015); this study	T23	3987	729.96	6.24
Negash Syncline	Swanson-Hysell et al. (2015); this study	T23	3989	729.91	5.47
Negash Syncline	Swanson-Hysell et al. (2015); this study	T23	3992.7	729.8	5.67
Negash Syncline	Swanson-Hysell et al. (2015); this study	T28	3825.9	734.66	4.48
Negash Syncline	Swanson-Hysell et al. (2015); this study	T28	3825.9	734.66	5.74
Negash Syncline	Swanson-Hysell et al. (2015); this study	T28	3825.9	734.66	5.74
Negash Syncline	Swanson-Hysell et al. (2015); this study	T28	3828.4	734.59	5.47
Negash Syncline	Swanson-Hysell et al. (2015); this study	T28	3828.4	734.59	4.84
Negash Syncline	Swanson-Hysell et al. (2015); this study	T28	3828.4	734.59	4.84
Negash Syncline	Swanson-Hysell et al. (2015); this study	T28	3830.6	734.52	6.71
Negash Syncline	Swanson-Hysell et al. (2015); this study	T28	3830.6	734.52	4.98
Negash Syncline	Swanson-Hysell et al. (2015); this study	T28	3830.6	734.52	6.71
Negash Syncline	Swanson-Hysell et al. (2015); this study	T28	3839	734.28	6.76
Negash Syncline	Swanson-Hysell et al. (2015); this study	T28	3839	734.28	6.14
Negash Syncline	Swanson-Hysell et al. (2015); this study	T28	3839	734.28	6.76
Negash Syncline	Swanson-Hysell et al. (2015); this study	T28	3843	734.16	6.45
Negash Syncline	Swanson-Hysell et al. (2015); this study	T28	3843	734.16	6.59
Negash Syncline	Swanson-Hysell et al. (2015); this study	T28	3843	734.16	6.59
Negash Syncline	Swanson-Hysell et al. (2015); this study	T28	3847.8	734.02	6.16
Negash Syncline	Swanson-Hysell et al. (2015); this study	T28	3847.8	734.02	7.4
Negash Syncline	Swanson-Hysell et al. (2015); this study	T28	3847.8	734.02	7.4
Negash Syncline	Swanson-Hysell et al. (2015); this study	T28	3848.7	733.99	6.79
Negash Syncline	Swanson-Hysell et al. (2015); this study	T28	3848.7	733.99	6.09
Negash Syncline	Swanson-Hysell et al. (2015); this study	T28	3848.7	733.99	6.79
Negash Syncline	Swanson-Hysell et al. (2015); this study	T28	3855.9	733.78	5.97
Negash Syncline	Swanson-Hysell et al. (2015); this study	T28	3855.9	733.78	6.33
Negash Syncline	Swanson-Hysell et al. (2015); this study	T28	3855.9	733.78	6.33
Negash Syncline	Swanson-Hysell et al. (2015); this study	T28	3862	733.61	4.97
Negash Syncline	Swanson-Hysell et al. (2015); this study	T28	3862	733.61	4.97
Negash Syncline	Swanson-Hysell et al. (2015); this study	T28	3862	733.61	5.28
Negash Syncline	Swanson-Hysell et al. (2015); this study	T28	3865.3	733.51	3.53
Negash Syncline	Swanson-Hysell et al. (2015); this study	T28	3865.3	733.51	3.53
Negash Syncline	Swanson-Hysell et al. (2015); this study	T28	3865.3	733.51	5.59
Negash Syncline	Swanson-Hysell et al. (2015); this study	T28	3875.7	733.21	5.64
Negash Syncline	Swanson-Hysell et al. (2015); this study	T28	3881.2	733.05	5.24
Negash Syncline	Swanson-Hysell et al. (2015); this study	T28	3885.4	732.93	5.64
Negash Syncline	Swanson-Hysell et al. (2015); this study	T28	3890.4	732.78	5.6
Negash Syncline	Swanson-Hysell et al. (2015); this study	T28	3898.9	732.53	6.43
Negash Syncline	Swanson-Hysell et al. (2015); this study	T28	3980.8	730.15	6.19
Negash Syncline	Swanson-Hysell et al. (2015); this study	T28	3980.8	730.15	4.27
Negash Syncline	Swanson-Hysell et al. (2015); this study	T28	3980.8	730.15	4.27
Negash Syncline	Swanson-Hysell et al. (2015); this study	T28	3982.5	730.1	6.46
Negash Syncline	Swanson-Hysell et al. (2015); this study	T28	3988.2	729.93	6.73
Negash Syncline	Swanson-Hysell et al. (2015); this study	T28	3991.5	729.83	6.48
Negash Syncline	Swanson-Hysell et al. (2015); this study	T28	3997.7	729.65	4.41
Negash Syncline	Swanson-Hysell et al. (2015); this study	T28	3997.7	729.65	4.41
Negash Syncline	Swanson-Hysell et al. (2015); this study	T28	3997.7	729.65	6.13
Negash Syncline	Swanson-Hysell et al. (2015); this study	T28	3998.7	729.62	5.98
Negash Syncline	Swanson-Hysell et al. (2015); this study	T28	4005	729.44	5.14
Negash Syncline	Swanson-Hysell et al. (2015); this study	T28	4010.8	729.27	3.74
Negash Syncline	Swanson-Hysell et al. (2015); this study	T37	3718.1	737.78	1.24

Negash Syncline	Swanson-Hysell et al. (2015); this study	T37	3722.1	737.71	-0.52
Negash Syncline	Swanson-Hysell et al. (2015); this study	T37	3723.1	737.69	0.47
Negash Syncline	Swanson-Hysell et al. (2015); this study	T37	3724.6	737.67	2.2
Negash Syncline	Swanson-Hysell et al. (2015); this study	T37	3726	737.65	1.26
Negash Syncline	Swanson-Hysell et al. (2015); this study	T37	3728	737.61	1.27
Negash Syncline	Swanson-Hysell et al. (2015); this study	T37	3729.8	737.58	0.54
Negash Syncline	Swanson-Hysell et al. (2015); this study	T37	3735.9	737.48	0.98
Negash Syncline	Swanson-Hysell et al. (2015); this study	T37	3737.2	737.46	1.45
Negash Syncline	Swanson-Hysell et al. (2015); this study	T37	3740.6	737.4	1.82
Negash Syncline	Swanson-Hysell et al. (2015); this study	T37	3742.2	737.38	1.89
Negash Syncline	Swanson-Hysell et al. (2015); this study	T37	3743.8	737.35	2.15
Negash Syncline	Swanson-Hysell et al. (2015); this study	T37	3744.5	737.34	2.4
Negash Syncline	Swanson-Hysell et al. (2015); this study	T37	3745.9	737.32	2.04
Negash Syncline	Swanson-Hysell et al. (2015); this study	T37	3747.8	737.28	1.84
Negash Syncline	Swanson-Hysell et al. (2015); this study	T37	3751.4	737.23	1.42
Negash Syncline	Swanson-Hysell et al. (2015); this study	T37	3752.5	737.21	1.12
Negash Syncline	Swanson-Hysell et al. (2015); this study	T37	3754.6	737.17	1.11
Negash Syncline	Swanson-Hysell et al. (2015); this study	T37	3755.7	737.15	0.44
Negash Syncline	Swanson-Hysell et al. (2015); this study	T37	3757.6	737.12	1.76
Negash Syncline	Swanson-Hysell et al. (2015); this study	T37	3758.9	737.1	0.81
Negash Syncline	Swanson-Hysell et al. (2015); this study	T37	3765.9	736.99	0.65
Negash Syncline	Swanson-Hysell et al. (2015); this study	T37	3766.9	736.97	0.86
Negash Syncline	Swanson-Hysell et al. (2015); this study	T37	3769	736.93	-1.21
Negash Syncline	Swanson-Hysell et al. (2015); this study	T37	3799.6	736.02	-5.4
Negash Syncline	Swanson-Hysell et al. (2015); this study	T37	3799.7	736.01	-5.05
Negash Syncline	Swanson-Hysell et al. (2015); this study	T37	3800.5	735.92	-4.78
Negash Syncline	Swanson-Hysell et al. (2015); this study	T37	3800.7	735.9	-4.21
Negash Syncline	Swanson-Hysell et al. (2015); this study	T37	3801.4	735.77	0.32
Negash Syncline	Swanson-Hysell et al. (2015); this study	T37	3801.7	735.71	-0.83
Negash Syncline	Swanson-Hysell et al. (2015); this study	T37	3802.4	735.58	1.81
Negash Syncline	Swanson-Hysell et al. (2015); this study	T37	3802.7	735.53	-0.89
Negash Syncline	Swanson-Hysell et al. (2015); this study	T37	3804.4	735.29	3.44
Negash Syncline	Swanson-Hysell et al. (2015); this study	T37	3805.3	735.26	1.94
Negash Syncline	Swanson-Hysell et al. (2015); this study	T37	3806.9	735.21	3.33
Negash Syncline	Swanson-Hysell et al. (2015); this study	T37	3808	735.18	4.54
Negash Syncline	Swanson-Hysell et al. (2015); this study	T37	3810.1	735.12	3.92
Samre Fold/Thrust Belt	this study	T40	3695.4	738.15	0.77
Samre Fold/Thrust Belt	this study	T40	3696.5	738.13	1.74
Samre Fold/Thrust Belt	this study	T40	3698.2	738.11	1.88
Samre Fold/Thrust Belt	this study	T40	3700.7	738.06	1.4
Samre Fold/Thrust Belt	this study	T40	3701.8	738.05	1.66
Samre Fold/Thrust Belt	this study	T40	3705.3	737.99	0.74
Samre Fold/Thrust Belt	this study	T40	3706.8	737.96	0.91
Samre Fold/Thrust Belt	this study	T40	3713.7	737.85	1.48
Samre Fold/Thrust Belt	this study	T40	3714.8	737.83	1.28
Samre Fold/Thrust Belt	this study	T40	3716.5	737.8	0.79
Samre Fold/Thrust Belt	this study	T40	3721.1	737.73	1.7
Samre Fold/Thrust Belt	this study	T40	3721.9	737.71	2.37
Samre Fold/Thrust Belt	this study	T40	3722.6	737.7	2.6
Samre Fold/Thrust Belt	this study	T40	3725.5	737.65	0.37
Samre Fold/Thrust Belt	this study	T40	3727.5	737.62	1.96
Samre Fold/Thrust Belt	this study	T40	3729.5	737.59	1.58
Samre Fold/Thrust Belt	this study	T40	3732.3	737.54	1.19
Samre Fold/Thrust Belt	this study	T40	3733.5	737.52	1.98
Samre Fold/Thrust Belt	this study	T40	3734	737.51	1.85
Samre Fold/Thrust Belt	this study	T40	3735.2	737.49	1.92
Samre Fold/Thrust Belt	this study	T40	3736.1	737.48	1.75
Samre Fold/Thrust Belt	this study	T40	3738.3	737.44	2.31
Samre Fold/Thrust Belt	this study	T40	3739.1	737.43	2.03
Samre Fold/Thrust Belt	this study	T40	3801.4	735.77	-3.53

Samre Fold/Thrust Belt	this study	T40	3808.1	735.18	4.13
Samre Fold/Thrust Belt	this study	T40	3809.4	735.14	3.94
Samre Fold/Thrust Belt	this study	T40	3810	735.12	4.72
Samre Fold/Thrust Belt	this study	T40	3810.8	735.1	4.9
Samre Fold/Thrust Belt	this study	T40	3811.7	735.07	5.56
Samre Fold/Thrust Belt	this study	T40	3813.7	735.01	5.99
Samre Fold/Thrust Belt	this study	T40	3815	734.98	5.97
Samre Fold/Thrust Belt	this study	T40	3816.9	734.92	6.28
Samre Fold/Thrust Belt	this study	T40	3818.5	734.87	5.2
Samre Fold/Thrust Belt	this study	T40	3819.3	734.85	6.36
Samre Fold/Thrust Belt	this study	T40	3821.1	734.8	7.06
Samre Fold/Thrust Belt	this study	T40	3821.7	734.78	7.02
Samre Fold/Thrust Belt	this study	T40	3823.3	734.73	6.85
Samre Fold/Thrust Belt	this study	T40	3824.3	734.71	7.04
Samre Fold/Thrust Belt	this study	T40	3825.6	734.67	7.22
Samre Fold/Thrust Belt	this study	T40	3826.6	734.64	7.15
Samre Fold/Thrust Belt	this study	T40	3828.3	734.59	5.27
Samre Fold/Thrust Belt	this study	T40	3829.4	734.56	7
Samre Fold/Thrust Belt	this study	T40	3829.7	734.55	7.07
Samre Fold/Thrust Belt	this study	T40	3830.7	734.52	6.6
Samre Fold/Thrust Belt	this study	T40	3832.6	734.46	7.18
Samre Fold/Thrust Belt	this study	T40	3838.8	734.28	5.79
Samre Fold/Thrust Belt	this study	T40	3839.7	734.26	5.56
Samre Fold/Thrust Belt	this study	T40	3841.1	734.22	5.68
Samre Fold/Thrust Belt	this study	T40	3842.8	734.17	5.67
Samre Fold/Thrust Belt	this study	T40	3844.6	734.11	4.18
Samre Fold/Thrust Belt	this study	T40	3847.2	734.04	5.94
Samre Fold/Thrust Belt	this study	T40	3848.6	734	5.51
Samre Fold/Thrust Belt	this study	T40	3849.1	733.98	5.54
Samre Fold/Thrust Belt	this study	T40	3851.9	733.9	5.44
Samre Fold/Thrust Belt	this study	T40	3854.5	733.83	4.61
Samre Fold/Thrust Belt	this study	T40	3858.1	733.72	5.96
Samre Fold/Thrust Belt	this study	T40	3861.1	733.63	4.5
Samre Fold/Thrust Belt	this study	T40	3862.2	733.6	5.34
Samre Fold/Thrust Belt	this study	T40	3863.6	733.56	5.68
Samre Fold/Thrust Belt	this study	T40	3868.1	733.43	4.12
Samre Fold/Thrust Belt	this study	T40	3870.9	733.35	6.02
Samre Fold/Thrust Belt	this study	T40	3875.9	733.2	5.72
Samre Fold/Thrust Belt	this study	T40	3880.3	733.07	6.64
Samre Fold/Thrust Belt	this study	T40	3881.7	733.03	6.6
Samre Fold/Thrust Belt	this study	T40	3884.2	732.96	6.46
Samre Fold/Thrust Belt	this study	T40	3886	732.91	6.45
Samre Fold/Thrust Belt	this study	T40	3888	732.85	6.73
Samre Fold/Thrust Belt	this study	T40	3889.7	732.8	6.72
Samre Fold/Thrust Belt	this study	T40	3892	732.73	6.8
Samre Fold/Thrust Belt	this study	T40	3894.8	732.65	6.61
Samre Fold/Thrust Belt	this study	T40	3897.3	732.58	6.7
Samre Fold/Thrust Belt	this study	T40	3899.5	732.51	6.89
Samre Fold/Thrust Belt	this study	T40	3901.3	732.46	6.1
Samre Fold/Thrust Belt	this study	T40	3903.2	732.41	5.82
Samre Fold/Thrust Belt	this study	T40	3905.7	732.33	6.52
Samre Fold/Thrust Belt	this study	T40	3907.1	732.29	6.44
Samre Fold/Thrust Belt	this study	T40	3909.2	732.23	6.65
Samre Fold/Thrust Belt	this study	T40	3911.7	732.16	6.89
Samre Fold/Thrust Belt	this study	T40	3912.8	732.13	7.26
Samre Fold/Thrust Belt	this study	T40	3916.1	732.03	6.89
Samre Fold/Thrust Belt	this study	T40	3917.9	731.98	7
Samre Fold/Thrust Belt	this study	T40	3918.8	731.95	6.43
Samre Fold/Thrust Belt	this study	T40	3920.2	731.91	6.25
Samre Fold/Thrust Belt	this study	T40	3921.6	731.87	7

Samre Fold/Thrust Belt	this study	T40	3924.1	731.8	6.89
Samre Fold/Thrust Belt	this study	T40	3925.7	731.75	7.11
Samre Fold/Thrust Belt	this study	T40	3927.2	731.71	7.09
Samre Fold/Thrust Belt	this study	T40	3927.3	731.7	7.08
Samre Fold/Thrust Belt	this study	T40	3927.3	731.7	6.82
Samre Fold/Thrust Belt	this study	T40	3929.7	731.63	5.27
Samre Fold/Thrust Belt	this study	T40	3929.7	731.63	6.55
Samre Fold/Thrust Belt	this study	T40	3932.3	731.56	6.68
Samre Fold/Thrust Belt	this study	T40	3932.3	731.56	6.83
Samre Fold/Thrust Belt	this study	T40	3933.2	731.53	6.95
Samre Fold/Thrust Belt	this study	T40	3935	731.48	6.86
Samre Fold/Thrust Belt	this study	T40	3935	731.48	5.86
Samre Fold/Thrust Belt	this study	T40	3936.3	731.44	5.84
Samre Fold/Thrust Belt	this study	T40	3937.4	731.41	4.91
Samre Fold/Thrust Belt	this study	T40	3938.2	731.39	5.16
Samre Fold/Thrust Belt	this study	T40	3939.5	731.35	5.12
Samre Fold/Thrust Belt	this study	T40	3942.5	731.26	6.53
Samre Fold/Thrust Belt	this study	T40	3944.7	731.2	6.51
Samre Fold/Thrust Belt	this study	T40	3944.7	731.2	6.36
Samre Fold/Thrust Belt	this study	T40	3945	731.19	6.45
Samre Fold/Thrust Belt	this study	T40	3945	731.19	6.54
Samre Fold/Thrust Belt	this study	T40	3947	731.13	6.61
Samre Fold/Thrust Belt	this study	T40	3948	731.1	6.91
Samre Fold/Thrust Belt	this study	T40	3951.2	731.01	6.51
Samre Fold/Thrust Belt	this study	T40	3952.7	730.96	6.75
Samre Fold/Thrust Belt	this study	T40	3955.6	730.88	6.66
Samre Fold/Thrust Belt	this study	T40	3957.2	730.83	6.38
Samre Fold/Thrust Belt	this study	T40	3957.2	730.83	6.46
Samre Fold/Thrust Belt	this study	T40	3957.6	730.82	6.13
Samre Fold/Thrust Belt	this study	T40	3957.6	730.82	5.08
Samre Fold/Thrust Belt	this study	T40	3959.9	730.75	6.51
Samre Fold/Thrust Belt	this study	T40	3959.9	730.75	6.36
Samre Fold/Thrust Belt	this study	T40	3960.9	730.72	6.68
Samre Fold/Thrust Belt	this study	T40	3960.9	730.72	6.42
Samre Fold/Thrust Belt	this study	T40	3962.1	730.69	4.41
Samre Fold/Thrust Belt	this study	T40	3962.1	730.69	3.81
Samre Fold/Thrust Belt	this study	T40	3964.3	730.63	4.34
Samre Fold/Thrust Belt	this study	T40	3965.6	730.59	4.66
Samre Fold/Thrust Belt	this study	T40	3965.6	730.59	5.9
Samre Fold/Thrust Belt	this study	T40	3967.7	730.53	3.53
Samre Fold/Thrust Belt	this study	T40	3967.7	730.53	4.72
Samre Fold/Thrust Belt	this study	T40	3969.8	730.47	4.53
Samre Fold/Thrust Belt	this study	T40	3973	730.37	2.27
Samre Fold/Thrust Belt	this study	T40	3973	730.37	3.93
Samre Fold/Thrust Belt	this study	T40	3974	730.34	4.61
Samre Fold/Thrust Belt	this study	T40	3974	730.34	4.14
Samre Fold/Thrust Belt	this study	T40	3976.4	730.27	4.06
Samre Fold/Thrust Belt	this study	T40	3976.5	730.27	5.89
Samre Fold/Thrust Belt	this study	T40	3976.5	730.27	5.46
Samre Fold/Thrust Belt	this study	T40	3977.7	730.24	5.35
Samre Fold/Thrust Belt	this study	T40	3977.7	730.24	6.11
Samre Fold/Thrust Belt	this study	T40	3979	730.2	5.29
Samre Fold/Thrust Belt	this study	T40	3980.1	730.17	4.97
Samre Fold/Thrust Belt	this study	T40	3980.1	730.17	5.61
Samre Fold/Thrust Belt	this study	T40	3981.3	730.13	5.6
Samre Fold/Thrust Belt	this study	T40	3981.3	730.13	5.45
Samre Fold/Thrust Belt	this study	T40	3982.4	730.1	5.98
Samre Fold/Thrust Belt	this study	T40	3982.4	730.1	5.37
Samre Fold/Thrust Belt	this study	T40	3983.9	730.05	4.41
Samre Fold/Thrust Belt	this study	T40	3984.9	730.03	4.96

Samre Fold/Thrust Belt	this study	T40	3985.8	730	4.7
Samre Fold/Thrust Belt	this study	T40	3987.3	729.96	5.48
Samre Fold/Thrust Belt	this study	T40	3988.6	729.92	4.64
Samre Fold/Thrust Belt	this study	T40	3988.6	729.92	4.68
Samre Fold/Thrust Belt	this study	T40	3988.8	729.91	5.64
Samre Fold/Thrust Belt	this study	T40	3988.8	729.91	4.62
Samre Fold/Thrust Belt	this study	T40	3990.5	729.86	5.08
Samre Fold/Thrust Belt	this study	T40	3991.5	729.83	5.3
Samre Fold/Thrust Belt	this study	T40	3992.6	729.8	5.16
Samre Fold/Thrust Belt	this study	T40	3993.8	729.77	5.12
Samre Fold/Thrust Belt	this study	T40	3995	729.73	4.85
Samre Fold/Thrust Belt	this study	T40	3996.6	729.68	4.68
Samre Fold/Thrust Belt	this study	T40	3997.7	729.65	5.16
Samre Fold/Thrust Belt	this study	T40	3999.7	729.59	5.81
Samre Fold/Thrust Belt	this study	T40	4001.9	729.53	6.09
Samre Fold/Thrust Belt	this study	T40	4002.8	729.5	5.7
Samre Fold/Thrust Belt	this study	T40	4005.1	729.44	5.56
Samre Fold/Thrust Belt	this study	T40	4007.7	729.36	4.44
Samre Fold/Thrust Belt	this study	T40	4008.4	729.34	4.52
Samre Fold/Thrust Belt	this study	T40	4009.4	729.31	4.47
Samre Fold/Thrust Belt	this study	T40	4011.4	729.25	4.4
Samre Fold/Thrust Belt	this study	T40	4018.3	729.05	4.21
Samre Fold/Thrust Belt	this study	T40	4020.1	729	4.55
Samre Fold/Thrust Belt	this study	T40	4022.1	728.94	3.33
Samre Fold/Thrust Belt	this study	T40	4022.1	728.94	3.41
Samre Fold/Thrust Belt	this study	T40	4024	728.89	4.18
Samre Fold/Thrust Belt	this study	T40	4026.1	728.83	3.41
Samre Fold/Thrust Belt	this study	T40	4027.6	728.78	5.41
Samre Fold/Thrust Belt	this study	T40	4029.3	728.73	2.43
Samre Fold/Thrust Belt	this study	T40	4031.1	728.68	5.13
Samre Fold/Thrust Belt	this study	T40	4034	728.59	5.14
Samre Fold/Thrust Belt	this study	T40	4034.6	728.58	4.65
Samre Fold/Thrust Belt	this study	T40	4036.8	728.51	5.45
Samre Fold/Thrust Belt	this study	T40	4036.8	728.51	2.74
Samre Fold/Thrust Belt	this study	T40	4037.6	728.49	3.92
Samre Fold/Thrust Belt	this study	T40	4039	728.45	4.02
Samre Fold/Thrust Belt	this study	T40	4041	728.39	3.45
Samre Fold/Thrust Belt	this study	T40	4043.2	728.33	3.58
Samre Fold/Thrust Belt	this study	T40	4044	728.3	1.49
Samre Fold/Thrust Belt	this study	T40	4044.1	728.3	3.34
Samre Fold/Thrust Belt	this study	T40	4044.6	728.29	3.72
Samre Fold/Thrust Belt	this study	T40	4045	728.27	2.37
Samre Fold/Thrust Belt	this study	T40	4045.8	728.25	3.66
Samre Fold/Thrust Belt	this study	T40	4047.3	728.21	4.16
Samre Fold/Thrust Belt	this study	T40	4048.9	728.16	4.24
Samre Fold/Thrust Belt	this study	T40	4050.1	728.13	4.17
Samre Fold/Thrust Belt	this study	T40	4051.6	728.08	3.23
Samre Fold/Thrust Belt	this study	T40	4051.9	728.07	4.39
Samre Fold/Thrust Belt	this study	T40	4051.9	728.07	3.39
Samre Fold/Thrust Belt	this study	T40	4053	728.04	6.06
Samre Fold/Thrust Belt	this study	T40	4054.5	728	5.59
Samre Fold/Thrust Belt	this study	T40	4055.9	727.96	5.77
Samre Fold/Thrust Belt	this study	T40	4056.9	727.93	5.74
Samre Fold/Thrust Belt	this study	T40	4057.7	727.9	5.56
Samre Fold/Thrust Belt	this study	T40	4058.3	727.89	6.13
Samre Fold/Thrust Belt	this study	T40	4059.3	727.86	4.67
Samre Fold/Thrust Belt	this study	T40	4064.6	727.7	5.34
Samre Fold/Thrust Belt	this study	T40	4065.6	727.67	5.19
Samre Fold/Thrust Belt	this study	T40	4068.5	727.59	5.35
Samre Fold/Thrust Belt	this study	T40	4069.5	727.56	5.23

Samre Fold/Thrust Belt	this study	T40	4070	727.55	5.23
Samre Fold/Thrust Belt	this study	T40	4070.7	727.53	5.3
Samre Fold/Thrust Belt	this study	T40	4072.5	727.47	5.24
Samre Fold/Thrust Belt	this study	T40	4073.5	727.44	5.14
Samre Fold/Thrust Belt	this study	T40	4075.6	727.38	3.7
Samre Fold/Thrust Belt	this study	T40	4075.9	727.37	3.64
Samre Fold/Thrust Belt	this study	T40	4079.8	727.26	5.24
Samre Fold/Thrust Belt	this study	T40	4080.7	727.23	5.14
Samre Fold/Thrust Belt	this study	T40	4082.1	727.19	5.42
Samre Fold/Thrust Belt	this study	T40	4083.4	727.16	4.97
Samre Fold/Thrust Belt	this study	T40	4085.8	727.09	5.08
Samre Fold/Thrust Belt	this study	T40	4087.6	727.03	5.26
Samre Fold/Thrust Belt	this study	T40	4089.7	726.97	4.32
Samre Fold/Thrust Belt	this study	T40	4092.6	726.89	4.86
Samre Fold/Thrust Belt	this study	T40	4093.5	726.86	4.77
Samre Fold/Thrust Belt	this study	T40	4094.2	726.84	4.63
Samre Fold/Thrust Belt	this study	T40	4095.9	726.79	4.8
Samre Fold/Thrust Belt	this study	T40	4096.9	726.76	4.56
Samre Fold/Thrust Belt	this study	T40	4099	726.7	4.19
Samre Fold/Thrust Belt	this study	T40	4100.3	726.66	4.53
Samre Fold/Thrust Belt	this study	T40	4104.6	726.54	2.02
Samre Fold/Thrust Belt	this study	T40	4106.3	726.49	1.88
Samre Fold/Thrust Belt	this study	T40	4106.85	726.47	2.03
Samre Fold/Thrust Belt	this study	T40	4131.9	725.74	4.89
Samre Fold/Thrust Belt	this study	T40	4133.2	725.7	6.58
Samre Fold/Thrust Belt	this study	T40	4134.4	725.67	6.19
Samre Fold/Thrust Belt	this study	T40	4135.6	725.63	5.8
Samre Fold/Thrust Belt	this study	T40	4137.9	725.57	5.37
Samre Fold/Thrust Belt	this study	T40	4139.9	725.51	5.43
Samre Fold/Thrust Belt	this study	T40	4140.7	725.49	4.23
Samre Fold/Thrust Belt	this study	T40	4141.5	725.46	6.38
Samre Fold/Thrust Belt	this study	T40	4142.8	725.42	5.95
Samre Fold/Thrust Belt	this study	T40	4146.2	725.33	5.21
Samre Fold/Thrust Belt	this study	T40	4146.9	725.3	5.98
Samre Fold/Thrust Belt	this study	T40	4149	725.24	5.94
Samre Fold/Thrust Belt	this study	T40	4151.1	725.18	7.14
Samre Fold/Thrust Belt	this study	T40	4151.7	725.17	6.31
Samre Fold/Thrust Belt	this study	T40	4152.5	725.14	6.53
Samre Fold/Thrust Belt	this study	T40	4153	725.13	5.32
Samre Fold/Thrust Belt	this study	T40	4155.1	725.07	4.37
Samre Fold/Thrust Belt	this study	T40	4156.2	725.03	3.63
Samre Fold/Thrust Belt	this study	T40	4157.3	725	5.66
Samre Fold/Thrust Belt	this study	T40	4158.5	724.97	7.02
Samre Fold/Thrust Belt	this study	T44	3781.1	736.73	0.65
Samre Fold/Thrust Belt	this study	T44	3800.5	735.92	-8.01
Samre Fold/Thrust Belt	this study	T44	3801.4	735.77	-8.32
Samre Fold/Thrust Belt	this study	T44	3809.6	735.13	-5.79
Samre Fold/Thrust Belt	this study	T44	3812.1	735.06	-6.63
Samre Fold/Thrust Belt	this study	T44	3821.9	734.78	3.92
Samre Fold/Thrust Belt	this study	T44	3823	734.74	2.6
Samre Fold/Thrust Belt	this study	T44	3824.3	734.71	5.97
Samre Fold/Thrust Belt	this study	T44	3825.1	734.68	6.52
Samre Fold/Thrust Belt	this study	T44	3827.1	734.62	6.45
Samre Fold/Thrust Belt	this study	T44	3829.6	734.55	5.26
Samre Fold/Thrust Belt	this study	T44	3831	734.51	6.18
Samre Fold/Thrust Belt	this study	T44	3833.4	734.44	5.05
Samre Fold/Thrust Belt	this study	T44	3835.7	734.37	5.65
Samre Fold/Thrust Belt	this study	T44	3836.2	734.36	6.61
Samre Fold/Thrust Belt	this study	T44	3837.2	734.33	6.18
Samre Fold/Thrust Belt	this study	T44	3838	734.31	6.17

Samre Fold/Thrust Belt	this study	T44	3838.7	734.29	6.45
Samre Fold/Thrust Belt	this study	T44	3840.2	734.24	3.43
Samre Fold/Thrust Belt	this study	T44	3840.9	734.22	3.85
Samre Fold/Thrust Belt	this study	T44	3880.5	733.07	3.39
Samre Fold/Thrust Belt	this study	T44	3882.9	733	4.6
Samre Fold/Thrust Belt	this study	T44	3884.3	732.96	3.02
Samre Fold/Thrust Belt	this study	T44	3886.2	732.9	2.04
Samre Fold/Thrust Belt	this study	T44	3889.4	732.81	4.18
Samre Fold/Thrust Belt	this study	T44	3891.9	732.74	4.2
Samre Fold/Thrust Belt	this study	T44	3893.2	732.7	3.18
Samre Fold/Thrust Belt	this study	T44	3894.2	732.67	4.36
Samre Fold/Thrust Belt	this study	T44	3897.5	732.57	4.89
Samre Fold/Thrust Belt	this study	T44	3899.6	732.51	5.09
Samre Fold/Thrust Belt	this study	T44	3902	732.44	4.74
Samre Fold/Thrust Belt	this study	T44	3906.3	732.32	5.08
Samre Fold/Thrust Belt	this study	T44	3909.2	732.23	5.07
Samre Fold/Thrust Belt	this study	T44	3909.2	732.23	5.73
Samre Fold/Thrust Belt	this study	T44	3911.4	732.17	5.73
Samre Fold/Thrust Belt	this study	T44	3916.8	732.01	4.06
Samre Fold/Thrust Belt	this study	T44	3931.9	731.57	5.09
Samre Fold/Thrust Belt	this study	T44	3940.5	731.32	4.35
Samre Fold/Thrust Belt	this study	T44	3947.1	731.13	6.61
Samre Fold/Thrust Belt	this study	T44	3955	730.9	6.71
Samre Fold/Thrust Belt	this study	T44	3963.2	730.66	6.68
Samre Fold/Thrust Belt	this study	T44	3987.9	729.94	5.64
Samre Fold/Thrust Belt	this study	T44	3999.1	729.61	4.32
Samre Fold/Thrust Belt	this study	T44	4015.3	729.14	2.9
Samre Fold/Thrust Belt	this study	T44	4033.6	728.61	5.71
Samre Fold/Thrust Belt	this study	T44	4035.3	728.56	4.37
Samre Fold/Thrust Belt	this study	T44	4046.5	728.23	4.8
Samre Fold/Thrust Belt	this study	T44	4058.3	727.89	5.27
Samre Fold/Thrust Belt	this study	T44	4062.1	727.78	2.66
Samre Fold/Thrust Belt	this study	T44	4066.9	727.64	3.16
Samre Fold/Thrust Belt	this study	T44	4078	727.31	4.85
Samre Fold/Thrust Belt	this study	T46	3703.6	738.02	1.82
Samre Fold/Thrust Belt	this study	T46	3704.5	738	1.6
Samre Fold/Thrust Belt	this study	T46	3706.2	737.97	0.1
Samre Fold/Thrust Belt	this study	T46	3708.3	737.94	1.09
Samre Fold/Thrust Belt	this study	T46	3709.5	737.92	2.19
Samre Fold/Thrust Belt	this study	T46	3710.4	737.9	0.98
Samre Fold/Thrust Belt	this study	T46	3711.1	737.89	1.44
Samre Fold/Thrust Belt	this study	T46	3712	737.88	0.92
Samre Fold/Thrust Belt	this study	T46	3713.4	737.85	2.35
Samre Fold/Thrust Belt	this study	T46	3714.4	737.84	0.79
Samre Fold/Thrust Belt	this study	T46	3716	737.81	1.75
Samre Fold/Thrust Belt	this study	T46	3716.6	737.8	2.34
Samre Fold/Thrust Belt	this study	T46	3717.6	737.79	0.77
Samre Fold/Thrust Belt	this study	T46	3719.4	737.76	1.23
Samre Fold/Thrust Belt	this study	T46	3720.8	737.73	-0.02
Samre Fold/Thrust Belt	this study	T46	3721.6	737.72	1.22
Samre Fold/Thrust Belt	this study	T46	3723.4	737.69	1.17
Samre Fold/Thrust Belt	this study	T46	3724.8	737.67	0.26
Samre Fold/Thrust Belt	this study	T46	3726.4	737.64	1.04
Samre Fold/Thrust Belt	this study	T46	3727.7	737.62	1.48
Samre Fold/Thrust Belt	this study	T46	3728.7	737.6	2.27
Samre Fold/Thrust Belt	this study	T46	3730.3	737.57	1.89
Samre Fold/Thrust Belt	this study	T46	3731.6	737.55	1.23
Samre Fold/Thrust Belt	this study	T46	3732.8	737.53	1.5
Samre Fold/Thrust Belt	this study	T46	3736	737.48	2.22
Samre Fold/Thrust Belt	this study	T46	3737.6	737.45	1.96

Samre Fold/Thrust Belt	this study	T46	3738.4	737.44	2.07
Samre Fold/Thrust Belt	this study	T46	3739.8	737.42	1.69
Samre Fold/Thrust Belt	this study	T46	3740.8	737.4	1.8
Samre Fold/Thrust Belt	this study	T46	3742.1	737.38	2.22
Samre Fold/Thrust Belt	this study	T46	3743.6	737.35	2.02
Samre Fold/Thrust Belt	this study	T46	3744.4	737.34	1.95
Samre Fold/Thrust Belt	this study	T46	3745.8	737.32	2
Samre Fold/Thrust Belt	this study	T46	3747.1	737.3	2.04
Samre Fold/Thrust Belt	this study	T46	3747.4	737.29	3.83
Samre Fold/Thrust Belt	this study	T46	3748.5	737.27	2.37
Samre Fold/Thrust Belt	this study	T46	3749.2	737.26	0.46
Samre Fold/Thrust Belt	this study	T46	3750.9	737.23	2.35
Samre Fold/Thrust Belt	this study	T46	3751.6	737.22	0.86
Samre Fold/Thrust Belt	this study	T46	3753	737.2	2
Samre Fold/Thrust Belt	this study	T46	3756.1	737.15	1.92
Samre Fold/Thrust Belt	this study	T46	3756.8	737.14	1.35
Samre Fold/Thrust Belt	this study	T46	3757.1	737.13	2.12
Samre Fold/Thrust Belt	this study	T46	3758.2	737.11	2.07
Samre Fold/Thrust Belt	this study	T46	3758.7	737.1	2.81
Samre Fold/Thrust Belt	this study	T46	3760.4	737.08	4.04
Samre Fold/Thrust Belt	this study	T46	3760.7	737.07	3.03
Samre Fold/Thrust Belt	this study	T46	3762.4	737.04	4.05
Samre Fold/Thrust Belt	this study	T46	3764	737.02	4.14
Samre Fold/Thrust Belt	this study	T46	3765	737	4.14
Samre Fold/Thrust Belt	this study	T46	3765.6	736.99	4.14
Samre Fold/Thrust Belt	this study	T46	3766.7	736.97	4.07
Samre Fold/Thrust Belt	this study	T46	3766.8	736.97	4.32
Samre Fold/Thrust Belt	this study	T46	3767.2	736.96	2.75
Samre Fold/Thrust Belt	this study	T46	3768.3	736.95	4.34
Samre Fold/Thrust Belt	this study	T46	3768.9	736.94	4.24
Samre Fold/Thrust Belt	this study	T46	3771	736.9	3.87
Samre Fold/Thrust Belt	this study	T46	3772.7	736.87	3.93
Samre Fold/Thrust Belt	this study	T46	3774.3	736.85	4.38
Samre Fold/Thrust Belt	this study	T46	3774.7	736.84	4.23
Samre Fold/Thrust Belt	this study	T46	3787.3	736.63	1.96
Samre Fold/Thrust Belt	this study	T46	3788	736.62	2.44
Samre Fold/Thrust Belt	this study	T46	3789.1	736.6	2.93
Samre Fold/Thrust Belt	this study	T46	3789.6	736.59	3
Samre Fold/Thrust Belt	this study	T46	3790.2	736.58	3.15
Samre Fold/Thrust Belt	this study	T46	3790.9	736.57	2.61
Samre Fold/Thrust Belt	this study	T46	3791.8	736.56	0.45
Samre Fold/Thrust Belt	this study	T46	3799.3	736.05	-3.29
Samre Fold/Thrust Belt	this study	T46	3799.7	736.01	-3.49
Samre Fold/Thrust Belt	this study	T46	3799.7	736.01	-4.23
Samre Fold/Thrust Belt	this study	T46	3801	735.84	-0.14
Samre Fold/Thrust Belt	this study	T46	3801.4	735.77	-0.02
Samre Fold/Thrust Belt	this study	T46	3802.8	735.51	-0.47
Samre Fold/Thrust Belt	this study	T46	3803.2	735.43	-1.29
Samre Fold/Thrust Belt	this study	T46	3803.9	735.3	-0.82
Samre Fold/Thrust Belt	this study	T46	3812.1	735.06	2.09
Samre Fold/Thrust Belt	this study	T46	3815	734.98	3.22
Samre Fold/Thrust Belt	this study	T46	3816.1	734.94	4.77
Samre Fold/Thrust Belt	this study	T46	3817.7	734.9	4.52
Samre Fold/Thrust Belt	this study	T46	3819.7	734.84	5.66
Negash Syncline	Swanson-Hysell et al. (2015); this study	T53	3749.1	737.26	0.44
Negash Syncline	Swanson-Hysell et al. (2015); this study	T53	3750	737.25	1.52
Negash Syncline	Swanson-Hysell et al. (2015); this study	T53	3750.6	737.24	1.63
Negash Syncline	Swanson-Hysell et al. (2015); this study	T53	3751.2	737.23	1.65
Negash Syncline	Swanson-Hysell et al. (2015); this study	T53	3752	737.22	1.43
Negash Syncline	Swanson-Hysell et al. (2015); this study	T53	3752.8	737.2	1.93

Negash Syncline	Swanson-Hysell et al. (2015); this study	T53	3753.6	737.19	2.03
Negash Syncline	Swanson-Hysell et al. (2015); this study	T53	3755.1	737.16	0.38
Negash Syncline	Swanson-Hysell et al. (2015); this study	T53	3755.7	737.15	1.64
Negash Syncline	Swanson-Hysell et al. (2015); this study	T53	3756.5	737.14	0.48
Negash Syncline	Swanson-Hysell et al. (2015); this study	T53	3756.8	737.14	-0.06
Negash Syncline	Swanson-Hysell et al. (2015); this study	T53	3757.6	737.12	-4.42
Negash Syncline	Swanson-Hysell et al. (2015); this study	T53	3802.1	735.64	-5.29
Negash Syncline	Swanson-Hysell et al. (2015); this study	T53	3802.6	735.54	-3.19
Negash Syncline	Swanson-Hysell et al. (2015); this study	T53	3803.1	735.45	-4.1
Negash Syncline	Swanson-Hysell et al. (2015); this study	T53	3803.8	735.32	-1.33
Negash Syncline	Swanson-Hysell et al. (2015); this study	T53	3804.3	735.29	0.61
Negash Syncline	Swanson-Hysell et al. (2015); this study	T53	3805.1	735.27	1.4
Negash Syncline	Swanson-Hysell et al. (2015); this study	T53	3806.1	735.24	1.41
Negash Syncline	Swanson-Hysell et al. (2015); this study	T53	3806.6	735.22	2.39
Negash Syncline	Swanson-Hysell et al. (2015); this study	T53	3807	735.21	3.98
Negash Syncline	Swanson-Hysell et al. (2015); this study	T53	3807.9	735.18	4.46
Negash Syncline	Swanson-Hysell et al. (2015); this study	T53	3808.5	735.17	4.53
Negash Syncline	Swanson-Hysell et al. (2015); this study	T53	3809.2	735.15	5.23
Negash Syncline	Swanson-Hysell et al. (2015); this study	T53	3809.7	735.13	5.43
Negash Syncline	Swanson-Hysell et al. (2015); this study	T53	3810.6	735.1	5
Negash Syncline	Swanson-Hysell et al. (2015); this study	T53	3811.5	735.08	5.57
Negash Syncline	Swanson-Hysell et al. (2015); this study	T53	3812.2	735.06	5.85
Negash Syncline	Swanson-Hysell et al. (2015); this study	T53	3812.9	735.04	5.93
Negash Syncline	Swanson-Hysell et al. (2015); this study	T53	3813.6	735.02	5.55
Negash Syncline	Swanson-Hysell et al. (2015); this study	T53	3814.7	734.99	6.24
Negash Syncline	Swanson-Hysell et al. (2015); this study	T53	3815	734.98	6.43
Negash Syncline	Swanson-Hysell et al. (2015); this study	T53	3816.8	734.92	6.51
Negash Syncline	Swanson-Hysell et al. (2015); this study	T53	3818.4	734.88	6.45
Negash Syncline	Swanson-Hysell et al. (2015); this study	T53	3821.4	734.79	6.69
Negash Syncline	Swanson-Hysell et al. (2015); this study	T53	3824.2	734.71	5.84
Negash Syncline	Swanson-Hysell et al. (2015); this study	T53	3828.8	734.57	6.75
Negash Syncline	Swanson-Hysell et al. (2015); this study	T53	3829.3	734.56	5.57
Samre Fold/Thrust Belt	this study	T63	3811.8	735.07	6.25
Samre Fold/Thrust Belt	this study	T63	3814.2	735	7.06
Samre Fold/Thrust Belt	this study	T63	3818.4	734.88	6.84
Samre Fold/Thrust Belt	this study	T63	3820.1	734.83	6.38
Samre Fold/Thrust Belt	this study	T63	3824.1	734.71	7.04
Samre Fold/Thrust Belt	this study	T63	3827.8	734.6	7.18
Samre Fold/Thrust Belt	this study	T63	3828.9	734.57	7.38
Samre Fold/Thrust Belt	this study	T63	3830.2	734.53	8.15
Samre Fold/Thrust Belt	this study	T63	3831.9	734.48	7.57
Samre Fold/Thrust Belt	this study	T63	3834.7	734.4	7.43
Samre Fold/Thrust Belt	this study	T63	3836.4	734.35	7.92
Samre Fold/Thrust Belt	this study	T63	3838.8	734.28	7.67
Samre Fold/Thrust Belt	this study	T63	3840.2	734.24	7.63
Samre Fold/Thrust Belt	this study	T63	3841.3	734.21	7.04
Samre Fold/Thrust Belt	this study	T63	3842.4	734.18	7.31
Samre Fold/Thrust Belt	this study	T63	3845.7	734.08	6.31
Samre Fold/Thrust Belt	this study	T63	3848.1	734.01	5.82
Samre Fold/Thrust Belt	this study	T63	3849.7	733.97	7.51
Samre Fold/Thrust Belt	this study	T63	3850.6	733.94	6.99
Samre Fold/Thrust Belt	this study	T63	3852.7	733.88	6.48
Samre Fold/Thrust Belt	this study	T63	3854	733.84	7.62
Samre Fold/Thrust Belt	this study	T63	3855.3	733.8	7.74
Samre Fold/Thrust Belt	this study	T63	3857.3	733.74	7.91
Samre Fold/Thrust Belt	this study	T63	3894.7	732.65	5.96
Samre Fold/Thrust Belt	this study	T63	3895.8	732.62	5.34
Samre Fold/Thrust Belt	this study	T63	3896.9	732.59	4.79
Samre Fold/Thrust Belt	this study	T63	3898.3	732.55	5.62
Samre Fold/Thrust Belt	this study	T63	3899.5	732.51	5.7

Samre Fold/Thrust Belt	this study	T63	3900.3	732.49	5.62
Samre Fold/Thrust Belt	this study	T63	3901.4	732.46	4.61
Samre Fold/Thrust Belt	this study	T63	3902.8	732.42	5.24
Samre Fold/Thrust Belt	this study	T63	3905.5	732.34	5.71
Samre Fold/Thrust Belt	this study	T63	3908.2	732.26	6
Samre Fold/Thrust Belt	this study	T63	3909.2	732.23	5.94
Samre Fold/Thrust Belt	this study	T63	3910.6	732.19	6.47
Samre Fold/Thrust Belt	this study	T63	3912.1	732.15	6.26
Samre Fold/Thrust Belt	this study	T63	3913.3	732.11	6.8
Samre Fold/Thrust Belt	this study	T63	3914.5	732.08	6.4
Samre Fold/Thrust Belt	this study	T63	3915.4	732.05	6.06
Samre Fold/Thrust Belt	this study	T63	3917.5	731.99	6.02
Samre Fold/Thrust Belt	this study	T63	3918.9	731.95	6.61
Samre Fold/Thrust Belt	this study	T63	3919.9	731.92	5.52
Samre Fold/Thrust Belt	this study	T63	3920.7	731.9	6.01
Samre Fold/Thrust Belt	this study	T63	3921.5	731.87	5.23
Samre Fold/Thrust Belt	this study	T63	3922.8	731.84	6.53
Samre Fold/Thrust Belt	this study	T63	3923.7	731.81	6.49
Samre Fold/Thrust Belt	this study	T63	3925.8	731.75	6.05
Samre Fold/Thrust Belt	this study	T63	3927.3	731.7	6.23
Samre Fold/Thrust Belt	this study	T63	3928.3	731.67	6.46
Samre Fold/Thrust Belt	this study	T63	3929.9	731.63	5.82
Samre Fold/Thrust Belt	this study	T63	3930.7	731.61	6.04
Samre Fold/Thrust Belt	this study	T63	3932.1	731.56	6.12
Samre Fold/Thrust Belt	this study	T63	3933.3	731.53	5.33
Samre Fold/Thrust Belt	this study	T63	3934.8	731.49	6.19
Samre Fold/Thrust Belt	this study	T63	3936	731.45	5.69
Samre Fold/Thrust Belt	this study	T63	3937.3	731.41	5.96
Samre Fold/Thrust Belt	this study	T63	3938.5	731.38	5.41
Samre Fold/Thrust Belt	this study	T63	3939.9	731.34	5.46
Samre Fold/Thrust Belt	this study	T63	3939.9	731.34	5.47
Samre Fold/Thrust Belt	this study	T63	3940.8	731.31	5.36
Samre Fold/Thrust Belt	this study	T63	3942.1	731.27	6.04
Samre Fold/Thrust Belt	this study	T63	3942.9	731.25	5.83
Samre Fold/Thrust Belt	this study	T63	3944	731.22	6.38
Samre Fold/Thrust Belt	this study	T63	3944.3	731.21	6.64
Samre Fold/Thrust Belt	this study	T63	3945.5	731.17	5.65
Samre Fold/Thrust Belt	this study	T63	3947	731.13	6.17
Samre Fold/Thrust Belt	this study	T63	3948.2	731.1	6.41
Samre Fold/Thrust Belt	this study	T63	3949.6	731.05	5.55
Samre Fold/Thrust Belt	this study	T63	3950.7	731.02	6.02
Samre Fold/Thrust Belt	this study	T63	3951.7	730.99	6.27
Samre Fold/Thrust Belt	this study	T63	3952.7	730.96	6.14
Samre Fold/Thrust Belt	this study	T63	3955.4	730.89	6.18
Samre Fold/Thrust Belt	this study	T63	3956.2	730.86	6.6
Samre Fold/Thrust Belt	this study	T63	3957	730.84	5.89
Samre Fold/Thrust Belt	this study	T63	3957.7	730.82	6.52
Samre Fold/Thrust Belt	this study	T63	3959	730.78	5.55
Samre Fold/Thrust Belt	this study	T63	3960.3	730.74	6.09
Samre Fold/Thrust Belt	this study	T63	3960.9	730.72	6.52
Samre Fold/Thrust Belt	this study	T63	3962.3	730.68	5.83
Samre Fold/Thrust Belt	this study	T63	3963.7	730.64	6.32
Samre Fold/Thrust Belt	this study	T63	3965.1	730.6	6.14
Samre Fold/Thrust Belt	this study	T63	3966.3	730.57	6.27
Samre Fold/Thrust Belt	this study	T63	3966.6	730.56	5.3
Samre Fold/Thrust Belt	this study	T63	3967.4	730.54	6.06
Samre Fold/Thrust Belt	this study	T63	3968.9	730.49	5.37
Samre Fold/Thrust Belt	this study	T63	3969.7	730.47	5.81
Samre Fold/Thrust Belt	this study	T63	3973.4	730.36	5.84
Samre Fold/Thrust Belt	this study	T63	3975.5	730.3	6.1

Samre Fold/Thrust Belt	this study	T63	3976.9	730.26	6.28
Samre Fold/Thrust Belt	this study	T63	3978.1	730.22	5.93
Samre Fold/Thrust Belt	this study	T63	3980.1	730.17	4.97
Samre Fold/Thrust Belt	this study	T63	3981.2	730.13	5.38
Samre Fold/Thrust Belt	this study	T63	3981.7	730.12	5.1
Samre Fold/Thrust Belt	this study	T63	3982.8	730.09	5.11
Samre Fold/Thrust Belt	this study	T63	3984.2	730.05	4.75
Samre Fold/Thrust Belt	this study	T63	3986.7	729.97	5.75
Samre Fold/Thrust Belt	this study	T63	3987.6	729.95	6.11
Samre Fold/Thrust Belt	this study	T63	3990.9	729.85	5.9
Samre Fold/Thrust Belt	this study	T63	3992.1	729.82	5.77
Samre Fold/Thrust Belt	this study	T63	3993.1	729.79	6.17
Samre Fold/Thrust Belt	this study	T63	3995.9	729.71	6.36
Samre Fold/Thrust Belt	this study	T63	3996.1	729.7	6.23
Samre Fold/Thrust Belt	this study	T63	3997.1	729.67	6.23
Samre Fold/Thrust Belt	this study	T63	3998.3	729.64	5.82
Samre Fold/Thrust Belt	this study	T63	3999.7	729.59	5.62
Samre Fold/Thrust Belt	this study	T63	3999.7	729.59	5.65
Samre Fold/Thrust Belt	this study	T63	4002.4	729.52	5.38
Samre Fold/Thrust Belt	this study	T63	4003.5	729.48	5.36
Samre Fold/Thrust Belt	this study	T63	4004.2	729.46	5.01
Samre Fold/Thrust Belt	this study	T63	4007.1	729.38	3.53
Samre Fold/Thrust Belt	this study	T63	4007.9	729.36	2.86
Samre Fold/Thrust Belt	this study	T63	4010.1	729.29	5.12
Samre Fold/Thrust Belt	this study	T63	4011.3	729.26	5.68
Samre Fold/Thrust Belt	this study	T63	4024.5	728.87	5.81
Samre Fold/Thrust Belt	this study	T63	4025.9	728.83	5.73
Samre Fold/Thrust Belt	this study	T63	4027.3	728.79	5.65
Samre Fold/Thrust Belt	this study	T63	4028.5	728.76	5.69
Samre Fold/Thrust Belt	this study	T63	4029.7	728.72	3.88
Samre Fold/Thrust Belt	this study	T63	4031.3	728.67	5.58
Samre Fold/Thrust Belt	this study	T63	4032.9	728.63	5.13
Samre Fold/Thrust Belt	this study	T63	4039.4	728.44	5.67
Samre Fold/Thrust Belt	this study	T63	4041.5	728.38	5.31
Samre Fold/Thrust Belt	this study	T63	4042.6	728.34	5.8
Samre Fold/Thrust Belt	this study	T63	4043.8	728.31	5.62
Samre Fold/Thrust Belt	this study	T63	4045	728.27	5.73
Samre Fold/Thrust Belt	this study	T63	4046.4	728.23	5.73
Samre Fold/Thrust Belt	this study	T63	4048	728.19	5.97
Samre Fold/Thrust Belt	this study	T63	4050.5	728.11	5.37
Samre Fold/Thrust Belt	this study	T63	4052.2	728.06	5.31
Samre Fold/Thrust Belt	this study	T63	4053.7	728.02	5.89
Samre Fold/Thrust Belt	this study	T63	4055.9	727.96	5.9
Samre Fold/Thrust Belt	this study	T63	4057.1	727.92	5.79
Samre Fold/Thrust Belt	this study	T63	4058.5	727.88	5.39
Samre Fold/Thrust Belt	this study	T63	4059.2	727.86	5.89
Samre Fold/Thrust Belt	this study	T63	4060.2	727.83	5.69
Samre Fold/Thrust Belt	this study	T63	4061.4	727.8	5.8
Samre Fold/Thrust Belt	this study	T63	4062.7	727.76	5.5
Samre Fold/Thrust Belt	this study	T63	4064.5	727.71	5.73
Samre Fold/Thrust Belt	this study	T63	4068	727.6	5.58
Samre Fold/Thrust Belt	this study	T63	4070.1	727.54	5.01
Samre Fold/Thrust Belt	this study	T63	4072.9	727.46	4.67
Samre Fold/Thrust Belt	this study	T63	4074.9	727.4	5.06
Samre Fold/Thrust Belt	this study	T63	4078.3	727.3	3.09
Samre Fold/Thrust Belt	this study	T63	4079.6	727.27	3.83
Samre Fold/Thrust Belt	this study	T63	4082.4	727.18	4.1
Samre Fold/Thrust Belt	this study	T63	4083.8	727.14	4.64
Samre Fold/Thrust Belt	this study	T63	4086.3	727.07	4.64
Samre Fold/Thrust Belt	this study	T63	4087.8	727.03	4.61

Samre Fold/Thrust Belt	this study	T63	4090.1	726.96	4.78
Samre Fold/Thrust Belt	this study	T63	4090.1	726.96	4.95
Samre Fold/Thrust Belt	this study	T63	4092	726.9	4.17
Samre Fold/Thrust Belt	this study	T63	4094.7	726.83	6.29
Samre Fold/Thrust Belt	this study	T63	4096.8	726.76	5.86
Samre Fold/Thrust Belt	this study	T63	4098.3	726.72	5.17
Samre Fold/Thrust Belt	this study	T63	4100.1	726.67	5.85
Samre Fold/Thrust Belt	this study	T63	4102.2	726.61	6.19
Samre Fold/Thrust Belt	this study	T63	4103.9	726.56	6.48
Samre Fold/Thrust Belt	this study	T63	4110.4	726.37	6.16
Samre Fold/Thrust Belt	this study	T63	4111.9	726.32	7.1
Samre Fold/Thrust Belt	this study	T63	4112.7	726.3	7.23
Samre Fold/Thrust Belt	this study	T63	4114.3	726.25	6.78
Samre Fold/Thrust Belt	this study	T63	4115.6	726.22	7.38
Samre Fold/Thrust Belt	this study	T63	4116.9	726.18	7.07
Samre Fold/Thrust Belt	this study	T63	4119.3	726.11	7.12
Samre Fold/Thrust Belt	this study	T63	4121.9	726.03	5.6
Samre Fold/Thrust Belt	this study	T63	4123.2	726	4.48
Samre Fold/Thrust Belt	this study	T63	4125.7	725.92	6.26
Samre Fold/Thrust Belt	this study	T63	4128.6	725.84	4.63
Samre Fold/Thrust Belt	this study	T63	4129.7	725.81	-0.13
Samre Fold/Thrust Belt	this study	T63	4179.2	724.36	2.11
Samre Fold/Thrust Belt	this study	T63	4180.6	724.32	3.09
Samre Fold/Thrust Belt	this study	T63	4183.7	724.23	2.25
Samre Fold/Thrust Belt	this study	T63	4185.6	724.18	2.72
Samre Fold/Thrust Belt	this study	T63	4186.8	724.14	2.66
Samre Fold/Thrust Belt	this study	T63	4187.8	724.11	2.59
Samre Fold/Thrust Belt	this study	T63	4190.6	724.03	1.92
Samre Fold/Thrust Belt	this study	T63	4191.7	724	1.59
Samre Fold/Thrust Belt	this study	T63	4196	723.87	0.91
Samre Fold/Thrust Belt	this study	T63	4197.4	723.83	1.48
Samre Fold/Thrust Belt	this study	T63	4204.6	723.62	1.12
Samre Fold/Thrust Belt	this study	T63	4206.4	723.57	2.06
Samre Fold/Thrust Belt	this study	T63	4214.6	723.33	3
Samre Fold/Thrust Belt	this study	T63	4216.9	723.27	3.04
Samre Fold/Thrust Belt	this study	T63	4218.4	723.22	3.1
Samre Fold/Thrust Belt	this study	T63	4219.8	723.18	3
Samre Fold/Thrust Belt	this study	T63	4223	723.09	3.35
Samre Fold/Thrust Belt	this study	T63	4225	723.03	3.1
Samre Fold/Thrust Belt	this study	T63	4226	723	3.29
Samre Fold/Thrust Belt	this study	T63	4227.4	722.96	3.39
Samre Fold/Thrust Belt	this study	T63	4228.7	722.92	3.38
Samre Fold/Thrust Belt	this study	T63	4231.5	722.84	3.07
Samre Fold/Thrust Belt	this study	T63	4235	722.74	2.87
Samre Fold/Thrust Belt	this study	T63	4237.8	722.66	2.75
Samre Fold/Thrust Belt	this study	T63	4240.6	722.57	3.4
Samre Fold/Thrust Belt	this study	T63	4242.7	722.51	2.92
Samre Fold/Thrust Belt	this study	T63	4243.2	722.5	2.99
Samre Fold/Thrust Belt	this study	T63	4247.4	722.38	3.84
Samre Fold/Thrust Belt	this study	T63	4249.8	722.31	3.39
Samre Fold/Thrust Belt	this study	T63	4255.3	722.15	3.49
Samre Fold/Thrust Belt	this study	T63	4261	721.98	3.88
Samre Fold/Thrust Belt	this study	T63	4263.2	721.92	3.78
Samre Fold/Thrust Belt	this study	T63	4267.4	721.79	3.75
Samre Fold/Thrust Belt	this study	T63	4270.1	721.71	3.69
Samre Fold/Thrust Belt	this study	T63	4274.6	721.58	4.11
Samre Fold/Thrust Belt	this study	T63	4277.4	721.5	4.26
Samre Fold/Thrust Belt	this study	T63	4279.1	721.45	3.76
Samre Fold/Thrust Belt	this study	T63	4281.9	721.37	3.78
Samre Fold/Thrust Belt	this study	T63	4284.4	721.3	3.61

Samre Fold/Thrust Belt	this study	T63	4289	721.16	3.8
Samre Fold/Thrust Belt	this study	T63	4289.9	721.14	4.06
Samre Fold/Thrust Belt	this study	T63	4293.3	721.04	3.94
Samre Fold/Thrust Belt	this study	T63	4297.5	720.92	3.78
Samre Fold/Thrust Belt	this study	T63	4300.7	720.82	3.83
Samre Fold/Thrust Belt	this study	T63	4304.1	720.72	3.3
Samre Fold/Thrust Belt	this study	T63	4306.3	720.66	3.06
Samre Fold/Thrust Belt	this study	T63	4309.1	720.58	3.77
Samre Fold/Thrust Belt	this study	T63	4311.9	720.5	3.91
Samre Fold/Thrust Belt	this study	T63	4314.1	720.43	3.41
Samre Fold/Thrust Belt	this study	T63	4316.2	720.37	3.94
Samre Fold/Thrust Belt	this study	T63	4318.9	720.29	3.91
Samre Fold/Thrust Belt	this study	T63	4321	720.23	3.84
Samre Fold/Thrust Belt	this study	T63	4324	720.14	4.03
Samre Fold/Thrust Belt	this study	T63	4327.9	720.03	4.11
Samre Fold/Thrust Belt	this study	T63	4330.9	719.94	4.15
Samre Fold/Thrust Belt	this study	T63	4334.5	719.84	3.74
Samre Fold/Thrust Belt	this study	T63	4337.1	719.76	3.61
Samre Fold/Thrust Belt	this study	T63	4340.1	719.68	3.51
Samre Fold/Thrust Belt	this study	T63	4342.5	719.61	3.64
Samre Fold/Thrust Belt	this study	T63	4342.5	719.61	3.68
Samre Fold/Thrust Belt	this study	T63	4344.9	719.54	2.63
Samre Fold/Thrust Belt	this study	T63	4349.8	719.39	3.24
Samre Fold/Thrust Belt	this study	T63	4352.4	719.32	2.95
Samre Fold/Thrust Belt	this study	T63	4355.5	719.23	0.33
Samre Fold/Thrust Belt	this study	T63	4358.1	719.15	3.14
Samre Fold/Thrust Belt	this study	T63	4360.7	719.07	2.48
Samre Fold/Thrust Belt	this study	T63	4366.4	718.91	2.67
Samre Fold/Thrust Belt	this study	T63	4369.2	718.83	2.83
Samre Fold/Thrust Belt	this study	T63	4372.6	718.73	3.15
Samre Fold/Thrust Belt	this study	T63	4382.1	718.45	2.53
Samre Fold/Thrust Belt	this study	T63	4383.2	718.42	2.56
Samre Fold/Thrust Belt	this study	T63	4385.8	718.34	2.57
Samre Fold/Thrust Belt	this study	T63	4399.9	717.93	2.37
Samre Fold/Thrust Belt	this study	T63	4401.5	717.89	2.41
Samre Fold/Thrust Belt	this study	T63	4402.7	717.85	2.46
Samre Fold/Thrust Belt	this study	T63	4404.1	717.81	2.45
Samre Fold/Thrust Belt	this study	T63	4407.3	717.72	1.59
Samre Fold/Thrust Belt	this study	T63	4407.8	717.7	1.99
Samre Fold/Thrust Belt	this study	T63	4409.4	717.66	2.39
Samre Fold/Thrust Belt	this study	T63	4410.8	717.61	2.31
Samre Fold/Thrust Belt	this study	T63	4412.8	717.56	2.45
Samre Fold/Thrust Belt	this study	T63	4414.1	717.52	2.02
Samre Fold/Thrust Belt	this study	T63	4416.5	717.45	2.5
Samre Fold/Thrust Belt	this study	T63	4417.9	717.41	2.09
Samre Fold/Thrust Belt	this study	T63	4419.2	717.37	2.19
Samre Fold/Thrust Belt	this study	T63	4423.6	717.24	1.2
Samre Fold/Thrust Belt	this study	T63	4424.8	717.21	1.53
Samre Fold/Thrust Belt	this study	T63	4426.2	717.17	1.83
Samre Fold/Thrust Belt	this study	T63	4428	717.11	2.21
Samre Fold/Thrust Belt	this study	T63	4429.2	717.08	1.93
Samre Fold/Thrust Belt	this study	T63	4430.6	717.04	2.45
Samre Fold/Thrust Belt	this study	T63	4431.9	717	2.24